Experiments concerning electron capture and loss to the continuum and convoy electron production by highly ionized projectiles in the 0.7—8.5-MeV/u range transversing the rare gases, polycrystalline solids, and axial channels in gold

M. Breinig, S. B. Elston, S. Huldt, L. Liljeby, C. R. Vane, S. D. Berry, G. A. Glass, M. Schauer, and I. A. Sellin
University of Tennessee, Knoxville, Tennessee 37916
and Oak Ridge National Laboratory, Oak Ridge, Tennessee 37830

G. D. Alton, S. Datz, and S. Overbury
Oak Ridge National Laboratory, Oak Ridge, Tennessee 37830

R. Laubert*
East Carolina University, Greenville, North Carolina 27834

M. Suter
Eidgenossische Technische Hochschule, 8093 Zürich, Switzerland
(Received 10 August 1981)

Velocity spectra of electrons emitted into the forward direction have been measured for 0.7—8.5-MeV/u projectile ions transversing He, Ne, and Ar targets, ploycrystalline solids (C, Al, Ag, Au), and axial channels in gold. Spectral shapes and yields are compared and contrasted with one another and with theories which seek to account for the cusp-shaped peaks observed in terms of electron capture and loss to low-lying projectile-centered continuum states. We report the results of both singles and coincidence measurements, where the dependence of cusp shapes and yields on the emergent-ion charge state are examined. For electron capture to the continuum (ECC), variance is noted with respect to the simple, first-order theory of Dettmann, Harrison, and Lucas. The ECC yields are compared to experimental and theoretical studies of bound-state capture, especially to high Rydberg states. For electron loss to low-lying continuum states (ELC), variance is noted with respect to the corresponding theories of Briggs, Drepper, and Day, and ELC cross sections are compared to total electron-loss cross sections. For convoy electron production in solids, no known theory accounts for the results. As in ELC processes, convoy cusp widths are observed to be velocity independent. Convoy electron yields are also observed to be independent of the emergent-ion charge state.

I. INTRODUCTION AND OVERVIEW OF RESULTS

A sharp cusp in the velocity spectrum of electrons, ejected in ion-atom and ion-solid collisions, is observed when the ejected electron velocity $\vec{v}_e$ matches that of the emergent ion $\vec{v}$ in both speed and direction. In ion-atom collisions, the electrons originate from capture to low-lying, projectile-centered continuum states (ECC) for fast bare or nearly bare projectiles, and from loss to those low-lying continuum states (ELC) when loosely bound projectile electrons are available. Most investigators now agree that ECC cusps are strongly skewed toward *lower* velocities, and exhibit full widths half maxima roughly proportional to v (neglecting target-shell effects, which are sometimes strong). A close examination of recent ELC data from our laboratory shows that ELC cusps are instead nearly *symmetric, with widths independent of v in the velocity range 6—18 a.u.*, a result not predicted by recent theory. In contrast, "convoy" electron cusps produced in heavy ion-solid collisions at MeV/u energies are slightly skewed toward *high* electron velocities, but exhibit velocity-independent widths very similar to ELC cusp widths. While the shape

of the convoy peaks is approximately independent of projectile Z, velocity, and of target material, we find that the yields in polycrystalline targets exhibit a strong dependence on projectile Z and velocity. While attempts have been made to link convoy electron production to binary ECC or ELC processes, sometimes at the last layer, or alternatively to a solid-state wake-riding model, our measured dependences of cusp shape and yield on projectile charge state and energy are inconsistent with the predictions of available theories.

When coincidence with emergent ion charge state q_e is required, ECC cusps can be sorted as to whether $0,1,2,\ldots$ additional bound-state captures occurred during the same collision which generated the continuum electron. Similarly, ELC cusps can be sorted as to how many additional electrons were lost. The shapes observed are relatively independent of whether or not additional capture or loss events occurred. The yields (production cross sections) tend to mimic the beam velocity, projectile Z, and projectile charge q dependence of corresponding single- and multiple-electron capture and loss cross sections.

For convoy electron production in solids, cusp shapes are again found to be independent of q_e. More remarkably, for polycrystalline and randomly oriented monocrystalline targets, the yields are found to be independent of q_e, i.e., to mirror the unweighted statistical fraction of emergent ions of each charge state even though there is an appreciable projectile Z dependence and reason to believe that the *observed* convoys originate in many cases well within one mean-free path for charge changing of the exit surface. For well-channeled ions, however, the convoy yield is strongly suppressed, pointing to the necessity of close approach to an atomic string in the bulk as a necessary precursor for convoy production.

Studies of ECC processes for bare ions on light atoms—H and He—especially at the highest velocities, are of particular importance. In recent articles[1] Shakeshaft and Spruch have focused attention on an unusual opportunity to test higher-order Born contributions to charge-transfer amplitudes. Moreover, strict scaling laws linking ECC studies using p, d, and alpha beams with corresponding studies using higher-Z bare projectiles should exist, and when derived should be subjected to experimental test by comparing the results for low-Z projectiles with the results for higher-Z bare projectiles in the same gas targets. At sufficiently high ion velocities, the mean charge state of an ion emergent from a solid also corresponds to $q_e \cong Z$. Thus also in the solid target case, scaling laws linking proton- or alpha-particle-induced convoy electron yields to those for higher-Z projectiles may be realizable.

Many of the results presented in this article have appeared in abbreviated form in the literature as referenced below, sometimes in letter format and sometimes in the form of more extended articles in other journals and proceedings. Our purposes in preparing this article for *Physical Review A* are as follows:

(i) to include new data and fuller discussion of previously published data than was possible in short communication format;

(ii) to provide a unified discussion of results which are scattered through journal proceedings not always as accessible as the *Physical Review A;*

(iii) to make comparison with data obtained in experiments using low-Z projectiles at ~ 100 keV/u transversing gases and solids and with corresponding theories.

This article has been postponed several times because new experimental results— especially those from coincidence experiments and from experiments using higher projectile velocities and charge states—significantly added to our understanding of the phenomena encountered. Some surprises continue to occur. While this article must therefore necessarily be seen as interim, in our opinion the volume of previously unreported or briefly reported results makes the publication of this more unified article advisable and of archival value.

II. HISTORY AND REVIEW OF PROGRESS THROUGH MID 1978

We paraphrase a review[2] of ECC, ELC, and convoy electron-production studies prepared in June 1978, amending it as needed to account for improved understanding of the experimental data as of that date.

A. Electron capture to the continuum (ECC)

Electron capture to the continuum describes capture to projectile-centered states, where the capture proceeds in analogy to electron transfer to bound states, but the wave function which describes the motion of the electron after the collision is instead a projectile-centered continuum wave function.

The phenomenon therefore represents a form of ionization, but one in which, for example, a plane-wave description of the captured electron is completely inappropriate. Rather, Coulomb waves centered on the projectile become a more appropriate description. Joseph Macek, in a series of publications with Eugene Rudd and others dating back to 1970,[3] makes the following analogy. Ionization can be thought of as the natural continuation of excitation to a sequence of orbits of ever-increasing principal quantum number into the continuum. The excitation cross sections continue smoothly right through the ionization limit, provided an appropriate normalization of continuum states *vis-à-vis* excitation to high-n Rydberg states per unit bandwidth Δn is considered. In like fashion, one may envision electron-capture events accompanying an ion-atom encounter into a sequence of orbits of ever-increasing principal quantum number n, whose production rate also continues smoothly from the region of high Rydberg states just below the continuum into the continuum. Somehow, this process went experimentally undiscovered and theoretically neglected during the 50-odd years which have elapsed since the initial development of the quantum theory. Although quantum-mechanical theories of excitation, ionization, and capture to bound states were worked out in the 1920's and 1930's, the electron-capture contribution to ionization was somehow ignored. That it can sometimes be extremely important is illustrated by a 1978 paper by Shakeshaft,[4] who finds that for certain energies ($\sim$40 keV), more than half the total cross section for ionization of hydrogen by protons is accounted for by this process. Understanding of the important interactions characterizing ion-atom, ion-molecule, and ion-solid encounters is thereby changed significantly.

It appears that the discussion of the electron-capture-to-continuum process initally arose in the course of attempting to explain orders of magnitude disagreements between experimental differential cross-section data and Born-approximation calculations in the ionization of He and H_2 by proton impact at angles $\sim 10°$ with respect to the forward direction. According to Macek's 1970 article[5] on the theory of the forward peak in the angular distributions of electrons ejected by fast protons, it was Rudd who elaborated a suggestion by Oldham[6] to explain the forward peaking by arguing that when the emitted electron is ejected at a velocity $\vec{v}_e$ near the projectile velocity $\vec{v}$, some electrons are subjected to a strong Coulomb drag in the forward direction before moving away from the proton as free electrons. Macek then devised a first-order approximation for the final-state wave function of the electron, proton, and residual ion which would describe an electron being "carried along" by a proton. He used an expansion of Faddeev's equations incorporating Green's functions for three noninteracting particles. To a first approximation Macek's expression for the ionization amplitude can be written

$$a = a_{\mathrm{DI}} + a_{\mathrm{ECC}} - a_p \ , \tag{1}$$

when a represents the total amplitude for electron ionization, a_{DI} represents the amplitude for direct ionization calculated in some approximation which does not account for strong projectile distortion, a_{ECC} is a "charge-exchange-to-continuum" amplitude which is dominant near $\vec{v}_e = \vec{v}$, and a_p is a counter term arising because the term with all outgoing particles described by plane waves has been counted twice. The final wave function of the electron in the ECC term, for example, can be represented as a Coulomb wave centered at the target. If $\vec{v}_e \cong \vec{v}$, then the electron has large momentum with respect to the target, and a Coulomb wave centered at the target describing this electron differs little from a plane wave. Therefore, the first and the third term approximately cancel. The ECC term becomes large and dominates. If $\vec{v}_e \ncong \vec{v}$, all three terms contribute and the cancelation is incomplete. According to Macek,[5] as elaborated by Duncan *et al.*[7] and Lucas and Macek,[7] interference effects are predicted to be observable when the phase of the ECC amplitude in Eq. (1) is varying rapidly owing to the Coulomb distortion of the final-state wave function, especially for small (but nonzero) angles for which the direct-ionization and charge-transfer amplitudes are comparable. Apart from the issue of interference effects, Macek's theory predicts an approximately symmetric distribution of electrons in velocity space centered at $\vec{v}_e = \vec{v}$, whose yield scales as Z^3.

In contrast, there exist several single-amplitude theories of the forward peak which seek to describe the $\vec{v}_e = \vec{v}$ peak through some enhancement factor multiplying a smoothly varying amplitude for direct ionization away from the forward peak, calculated, for example, in Born approximation to first or second order. The best known of these are due to Salin[8] and to Dettmann, Harrison, and Lucas.[9] Working within the framework of a first Born approximation to ionization, Salin devised an approximate scheme for introducing projectile dis-

tortion of the continuum electron wave function over and above the more usual allowance for target distortion. As discussed in a recent comment by Ponce and Meckbach,[10] the final state may be thought of as a two-center continuum molecular orbital. Salin's distorted-wave approximation leads to one-center continuum atomic orbitals about the appropriate nucleus for electrons slow with respect to one of the nuclei, while describing the electron in the combined-atom continuum when the electron is fast with respect to both heavy particles. As discussed by Rødbro and Andersen,[11] Salin's theory predicts an asymmetric peak in the velocity spectrum of ejected electrons at low projectile velocities, which tends toward symmetry at high velocities because of the underlying shape of the Born cross section, a prediction unfulfilled either in the data of Ref. 11 or in our data. Obviously, no interference can occur in this or any other single-amplitude theory.

The theory of Dettmann *et al.* explicitly considers charge transfer to the continuum to be the dominant process in the production of $\vec{v}_e \cong \vec{v}$ electrons, which are represented in terms of projectile-centered Coulomb waves. The structure developed for the T matrix describing the scattering has a very similar form to that for bound-state capture, except that a continuum-state wave function replaces a bound-state wave function in the final state.

A singularity in the Coulomb wave-normalization factor $e^{\eta\pi/2}\Gamma(1+i\eta)$, can be viewed as the origin of a divergence of the differential cross section at zero degrees.

The continuum Coulomb wave function can be written

$$\Psi_{\vec{k}}(\vec{r}) = (2\pi)^{-3/2} e^{\eta\pi/2}\Gamma(1+i\eta) e^{i\vec{k}\cdot\vec{r}} \times {}_1F_1[-i\eta, 1, -i(kr+\vec{k}\cdot\vec{r})] , \tag{2}$$

where $k = |\vec{k}|$, $\vec{k} = (m/\hbar)(\vec{v}_e - \vec{v})$, and $\eta \equiv Z/(a_0 k)$.

Dettmann *et al.* made the approximation $\eta >> 1$ or

$$e^{\eta\pi}|\Gamma(1+i\eta)|^2 = \frac{2\pi\eta}{1-e^{-2\pi\eta}} \cong 2\pi\eta \equiv f(k) . \tag{3}$$

The form derived for the differential cross section is

$$\frac{d\sigma}{d\vec{v}_e} = f(k)F(v) . \tag{4}$$

If this form is integrated over a cone of half angle θ_0 centered on the forward direction, the result obtained is (in the notation of Ref. 1, except $Z = Z_B$, Z_T = target Z)

$$\frac{d\sigma_{\mathrm{BK}}}{dv_e}(1s \to \text{continuum}) \cong \frac{2^{17}}{5} Z_T^5 Z^3 \left[\frac{e^2}{\hbar v}\right]^{10} \left[\frac{1}{v^2}\right] \{[(v_e - v)^2 + (v\theta_0)^2]^{1/2} - |v_e - v|\} \pi a_0^2$$
$$= 4\pi^2 Z F_{\mathrm{BK}}(v) \left[\frac{e^2}{\hbar}\right] \{[(v_e - v)^2 + (v\theta_0)^2]^{1/2} - |v_e - v|\} , \tag{5}$$

$$F_{\mathrm{BK}}(v) = \frac{2^{16}}{10\pi^2} \frac{Z^2 Z_T^5}{(e^2/\hbar)^3} \left[\frac{e^2}{\hbar v}\right]^{12} \pi a_0^2 . \tag{6}$$

In an attempted further refinement, their second-order Born estimate of F leads to

$$F_{\mathrm{BK}} \to F(v) \cong F_{\mathrm{BK}}[0.3 + Q(v^{-1})] . \tag{7}$$

In this theory the assertion is that $f = f(k)$, *not* $f(\vec{k})$, i.e., isotropy in the projectile rest frame is predicted. Put another way, as in the BK approximation to bound-state capture, capture to s states is predicted to dominate at high velocities. The asymmetry of all ECC cusps measured in our work conflicts with this view.

The theory of Dettmann *et al.* applies when the projectile velocity v is much greater than v_0, the initial velocity of the electron to be captured in the target (i.e., the approximation $v_0 \cong 0$ is made). Our data exhibit strong target-shell effects if the condition $v >> v_0$ is not well satisfied.

The pioneering experimental work on ECC was done by Crooks and Rudd[12] for fast protons on He. A process identified as ECC (CEC for charge exchange to the continuum, in their parlance) by Lucas and collaborators was discovered at nearly the same time by Dettmann, Harrison, and Lucas[9] in experiments on fast protons emergent from C foils. We would instead characterize these $\vec{v}_e = \vec{v}$ electrons as convoy electrons, whose origin we believe cannot be described by a simple ECC (CEC)

mechanism (at least not for the fast, highly ionized projectiles in the range 6—18 a.u. used in our work).

At the time of the 1978 review, Lucas had also continued work with other collaborators,[9,13–15] for various H and He projectiles, mostly in thin solid and occasionally in gas targets, at projectile energies up to 1.2 MeV/u. Extensive work with both solid and gas targets and H and He projectiles had been undertaken by Menendez, Duncan, and coworkers[16] and with solid targets by Meckbach *et al.*[17] The latter authors prepared two summary articles[17] which emphasized several controversial disagreements between the various data and the theoretical predictions discussed so far for ECC as of 1977.

Chiu, McGowan, and Mitchell[18] extended the work of Meckbach *et al.*[17] to gas targets and found support for an ECC description in gas targets, in opposition to the alleged deficiencies of such a description for solid targets, as found in the latter work. Soon thereafter Stecklemacher *et al.*[19] criticized the interpretation given the data of Meckbach *et al.* on instrumental resolution and background treatment grounds, and argued for the validity of the ECC (CEC) model for the solid-target case as well. They also argued against a rival, solid-state "wake-riding" description of convoy electron production in solid targets.[20] The latter model considered the possibility that electrons may be trapped in an oscillatory, electron-density polarization potential extending behind and moving with the projectile, finally being liberated at the exit surface.

In the ion-atom collision case for 0.7-MeV/u d^+ projectiles on Ar we confirmed, apart from a measurable asymmetry, that the cusp shapes agreed approximately with those predicted by Dettmann *et al.*, as had been earlier established by Cranage and Lucas.[14] However, Cranage and Lucas had subtracted a large background attributed to the direct ionization.

While at the time we were puzzled to find much smaller backgrounds than those of Cranage and Lucas, we believe subsequent results suggest that their early results suffered from spurious backgrounds of unexplained origin, now reduced or absent with their more recently developed electron spectrometric apparatus.[21]

The question of whether and how to subtract backgrounds underneath the cusps is fundamental. A convincing argument was made by Rudd and Macek[3] and subsequently by many others that no unambiguous subtraction of electrons due to direct, target-centered ionization processes from those due to projectile-centered ECC processes can be made. Essentially, one argues that electrons reaching particular energy-momentum continuum states are physically indistinguishable, and the decision as to which mechanism operates to produce a specific electron cannot be made even in principle.

As we have seen, a significant prediction of the theory of Dettmann *et al.* and also that of Macek is a Z^3 dependence for $d\sigma/dv_e$ for a given projectile v. We did *not* find this dependence in the observed cross-section ratio (when integrated between suitably scaled, fixed velocity limits) for bare O^{8+} vs C^{6+} ions tranversing Ar gas at the same velocity. However, this ratio was found to be independent of velocity, just as predicted.

In Fig. 1, taken from Ref. 22, the cusp cross section (arbitrary scale) integrated over electron velocity between fixed but scaled velocity limits is plotted for bare C^{6+} and O^{8+} ions in Ar versus energy per nucleon, on a logσ vs logE/A plot. The fact that the curves are parallel shows both a common velocity dependence and a velocity-independent Z dependence. Integrating $d\sigma(\theta_0)/dv_e$ between the velocity limits $(1-\alpha)v$ and $(1+\alpha)v$, where α is arbitrary but consistently chosen to be 0.04, standardizes a fixed, scaled velocity-interval region of integration, which scales as theoretically predicted by Dettmann *et al.*[9] and minimizes background and shape corrections. Directly measured O^{8+}/C^{6+} yield ratios at 1.88 and 2.50 MeV/u give approximately 1.87 ± 0.08 and 1.94 ± 0.08, corresponding to predicted ratios of 2.37 if a Z^3 dependence is assumed. Our results are consistent with a $Z^{2.3\pm0.3}$ power law. The error bars correspond to range errors in the measured ratios. Apart from the asymmetry there is reasonably good agreement between theory and experiment concerning cusp

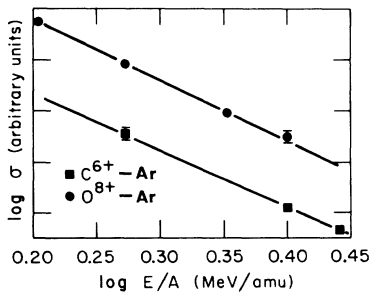

FIG. 1. Z and v dependence of electron capture into continuum states for bare C^{6+} and O^{8+} ions in a logσ vs logE/A power-law plot.

widths. Following an unpublished suggestion of Macek that the integration limits might be too broad, opening the possibility of a mixed-Z power in the range $Z=6-8$, we varied the region of integration, but found no systematic change in the power over the entire range $\alpha=0.01-0.04$. We also carried out previously unpublished measurements for deuterons and bare Si^{14+} ions in Ar at the same velocities. The same $Z^{2.3\pm0.3}$ power law is found to correctly predict both the $d+Ar$ and $Si^{14+}+Ar$ cross sections, within error bars.

The dependence of the cusp yields on projectile velocity was also established. Least-squares fits to the experimental exponent in v^{-n} yielded $n=4.55\pm0.19$ and $n=4.65\pm0.14$ for C^{6+} and O^{8+}, respectively, where standard errors in the fits are indicated, and are much weaker than the v^{-10} dependence of Eq. (5). In these experiments, asymptotically high velocities had not been reached. These exponents are in fact very similar to those fitted to the corresponding bound-state electron-capture cross sections measured by MacDonald and Martin[23] for the same projectile-target combination at overlapping velocities.

Though their results were not yet published at the time of the 1978 review, and hence not generally available then, Rødbro and Andersen[11] had submitted a paper concerning ECC for 0.015–1.5-MeV/u H^+ in He, Ar, and H_2, which is discussed in this section. They studied doubly differential ECC cross sections $d^2\sigma/dE\,d\Omega$, as well as yields, using a parallel-plate electrostatic analyzer with energy resolution $\Delta E/E$ of 1% FWHM and a collection cone of half-angle $\theta_0\cong6.3\times10^{-3}$ rad. A sharp maximum was found in the cross sections for $v\sim1.4v_0$, where v_0 is the initial velocity of the target electron captured. In accord with our results, the decrease of the cross section with increasing proton velocities resembles that for capture to bound states in the same collision system. Shell effects were seen for Ne and Ar, a result again in good accord with the findings we present for our higher-Z, higher-v data in Sec. IV. A reduced cross section σ_c was extracted from the data and compared to capture-to-excited-state measurements of other investigators. It was derived by extrapolating ECC cross sections to bound-state capture cross sections into Rydberg states across the ionization limit according to $\sigma_n=n^{-3}\sigma_c$ in accordance with the recipe originally proposed by Rudd and Macek. The agreement is remarkably good (there appears to be a 25% analysis error we comment upon in Sec. IV).

Unfortunately, Rødbro and Andersen chose to quote cross-section data after subtraction of a smooth background as in Fig. 2, which is taken from their paper. We have argued that background subtraction, apart from spurious background signals reaching the detector from unrelated or secondary processes, is improper. Fortunately for the most part the errors introduced are seen to be modest over the greater part of the energy range used, so that their quoted data would appear still to have considerable value.

Figure 3 displays a comparison of absolute differential cross-section measurements for H^+ in Ar we made using proton and deuterium beams at overlapping velocities with Rødbro and Andersen's absolute differential cross sections,[11] using the same, probably erroneous, background-treatment procedure. (We provide corrected values in Sec. IV.)

Both cross-section values have been rendered absolute by calibrating the apparatus with respect to absolute cross-section measurements for Ar L-shell Auger electron production in the range 158–212 eV by Stolterfoht *et al.*[24] From the work of Rudd[25] it is known that these cross sections are

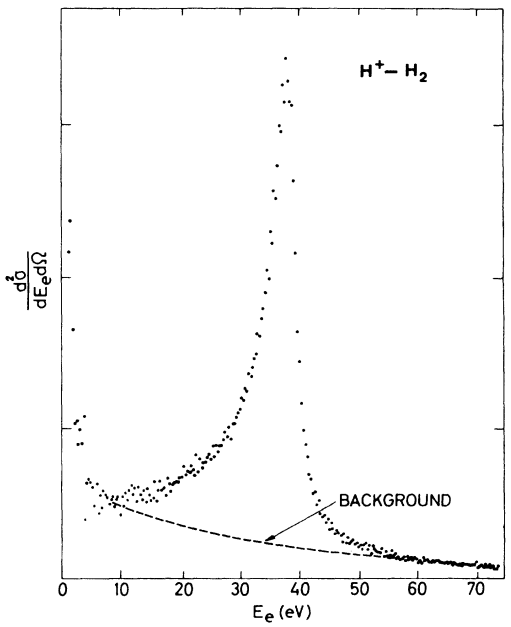

FIG. 2. The doubly differential cross section for protons in H_2 from data as measured by Rødbro and Andersen (Ref. 11). The fitted background under the forward peak is shown. When calculating the singly differential cross section, or forward peak yield, only the peak area above this background was evaluated.

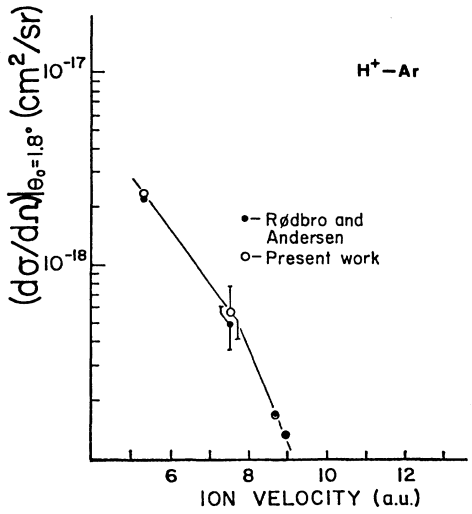

FIG. 3. Comparison of absolute differential cross sections for H^+-Ar from present work and results of Ref. 11.

nearly isotropic (to within $\sim 10\%$).

Figure 3 demonstrates excellent consistency of the cross-section scales used by Rødbro and Andersen and by us; in fact, the agreement is fortuitously good (note that both cross-section scales need modification to account for the probably improper subtraction made in Ref. 11). The absolute cross sections are estimated by Rødbro and Andersen to be correct to better than 25%, and the relative errors to be less than 10%. We are inclined to view these error bars as optimistic for two reasons:

(1) The so-called "background" subtracted in their analysis should probably be included in the cross section.

(2) The singly differential cross section $d\sigma/d\Omega$ is averaged over a finite solid angle $\Delta\Omega$. If the electron-velocity distribution is sharply peaked then a slight pointing error such that the acceptance cone of the analyzer is not exactly centered at 0°, introduces an error in $d\sigma/d\Omega$. This error is larger if the electron-velocity distribution is asymmetric. The asymmetry of ECC cusps is now well established and arises in part from a discontinuity in the doubly differential cross section for ECC when viewed in the projectile rest frame because contributions from higher partial waves (for example, p waves) become important. Furthermore $\Delta\Omega$ was chosen differently by Rødbro and Andersen and by us.

As will be shown in Sec. IV, our absolute cross-section errors are estimated at 40%. Whenever error bars appear in this paper, they represent one standard-deviation error in the range of repeated measurements. These relative errors are typically smaller than 40%.

B. Electron loss to the continuum (ELC)

When partially ionized projectiles undergo ion-atom collisions, it is now well known[22,26–28] that a superficially similar peak in the velocity spectrum of electrons emitted in the forward direction arises from projectile ionization, and that cross sections for ELC dominate whenever loosely bound projectile electrons are available. Though the "C" in the ELC may seem redundant, its use reminds us of parallel ECC phenomena and further reminds us that electron loss from heavy particles (usually targets) can occur through electron capture by the binary collision partner, thereby liberating no electrons in the continuum.

At the time of the 1978 review, Drepper and Briggs[26] had published a theory concerning binary-collisional electron loss by fast projectile ions in which the laboratory-frame velocity distribution of the forward ejected electrons displays a sharp cusp in both energy and angle centered near $\vec{v}_e = \vec{v}$. The theoretical cusp shape closely resembles that predicted in the theories of Dettmann, Harrison, and Lucas,[9] Salin,[8] and Macek[5] for the forward peak in electron-capture-to-continuum states (ECC) by bare ions for the very good reason that the same Coulomb factor appears in the differential cross section for ECC and ELC.

Menendez *et al.*[16] performed the prototype charge-state-variation experiment, in comparing electron spectra for He^+ and He^{2+} on Ar, finding no significant differences in the cusp shapes. In two other studies of ELC vs ECC cusp shapes for He^+ and He^{2+} on He, Lucas *et al.*[15] confirmed that the shapes are highly similar, while Meckbach *et al.*[29] find symmetric, narrower cusps for He^+ projectiles implying that ELC is an important electron-production mechanism.

The latter observation is entirely in accord with our 1978 observation of ELC.[28,30] Figure 4 reproduces data from Ref. 28. The figure shows energy spectra obtained for electrons emitted in the forward direction using an argon gas target and O^{q+} and Si^{q+} projectile ions. All spectra displayed are for projectiles having the same velocity (2.5 MeV/u). Each of the spectra has been normalized to the same peak height and no analyzer-transmission or detection efficiency corrections have been made. The uppermost two spectra are

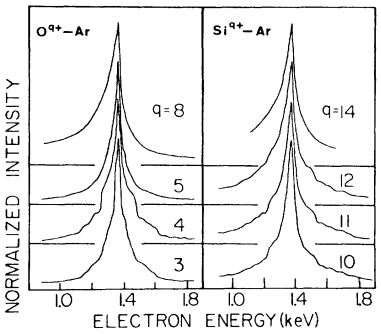

FIG. 4. Normalized spectra for electron capture and loss to continuum states in the forward direction for 2.5-MeV/u O^{q+} and Si^{q+} on Ar. Zero-count base lines are shown for each spectrum. Statistical errors are about 2% at the peaks.

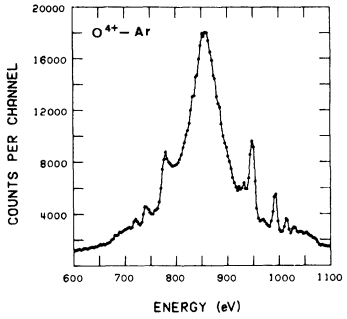

FIG. 5. Energy spectrum of electrons emitted in the forward direction in collisions of 25-MeV O^{4+} on Ar.

ECC spectra for bare O^{8+} and Si^{14+} and exhibit the typical skewed distribution found previously by us[22] for ECC by bare ions. A much more symmetric, narrower, and almost structureless cusp is shown for O^{5+} projectiles in Ar. The absolute yield, obtained by numerically integrating the cusp over the velocity interval v (1 ± 0.04), is about 2.2 times greater for O^{5+} than for O^{8+} projectiles. The contribution of ECC to the cusp produced by O^{5+} projectiles can be estimated assuming an effective-ion charge of $Z_{\rm eff}=q$ and scaling the known O^{8+} yield by $Z_{\rm eff}^{2.3}$. We had previously confirmed this single-power $Z^{2.3}$ scaling for the bare ions C^{6+}, O^{8+}, and Si^{14+} in the energy range 1.6–3.9 MeV/u. Subtracting the ECC contribution from the absolute cusp yields shows that for 1.6–2.5-MeV/u O^{q+} projectiles the ELC yield dominates the ECC yield when L-shell electrons are present. For O^{5+} at 2.5 MeV/u on Ar, the ELC contribution is about four times the ECC contribution. Thus the narrower, more symmetric, and therefore significantly different peaks observed for O^{5+}, O^{4+}, and O^{3+} vs O^{8+} projectiles are indicative of ELC processes. The variation in the peak shape is similar for Si^{q+} projectiles.

The symmetric maxima and minima appearing in the cusp wings in Fig. 4 originally misled us into seeking a description of the observed structure in terms of interference, which as noted above has been predicted but not found for ECC and has not been predicted for ELC. Much of the interpretive discussion in Ref. 28 (and repeated in Ref. 2) is therefore obsolete. The real origin of the observed structures was revealed in new measurements at lower velocities and was published very shortly thereafter in Ref. 30. Since no single-electron excitation can lead to autoionization lines in the energy ranges in question, autoionization was initially considered improbable as a source of the observed structures. Nevertheless, double-electron excitations proved to be responsible. Lower projectile energy and improved energy resolution showed that the structures found earlier form a Rydberg series of intense lines. These lines can be assigned to doubly excited autoionizing states of the projectile instead of the two-electron continuum states conjectured previously. The apparatus and methods employed in this work were similar to those used earlier, but instead of a spherical-sector analyzer a parallel-plate analyzer was employed to analyze electrons emitted near zero degrees. The acceptance angles of this spectrometer were kept smaller than 0.5°, producing an energy resolution of about 0.7% (FWHM). Spectra were collected for C^{2+} and O^{4+} projectiles at energies between 0.5 and 1.56 MeV/u using Ar as the target gas. In all spectra at least three resolved lines have been observed in each wing of the cusp. A representative spectrum is shown in Fig. 5. A series of lines is visible in both wings of this cusp. These lines originate from $(1s^2 2pnl)$ projectile autoionizing states.

In the projectile rest frame the energies of these lines correspond to the following series of transitions: $(1s^2 2pnl)\rightarrow(1s^2 2s)+e^-(k,l')$. For doubly excited C^{2+}, projectile rest frame energies of 2.7 ± 0.2, 4.2 ± 0.3, 5.2 ± 0.3 eV, ... were measured, corresponding to $n=5,6,7,\ldots$; for O^{4+}, energies of 2.1 ± 0.2, 4.7 ± 0.3, 6.3 ± 0.3 eV, ... were measured ($n=6,7,8,\ldots$). The energies of the ejected electrons are accurately predicted by the simple formula $E=E_\infty-(13.6q^2)/(n-\mu)^2$, where E_∞ is the energy in eV of the series limit, q is the charge of the residual ion, n is the principal quantum number of an electron in a Rydberg autoionizing state, and μ is the quantum defect. The values for

E_∞ can be taken from atomic energy-level tables,[31] and are 8.00 eV for carbon and 11.98 eV for oxygen. The experimental E values can be made to agree with calculated values within error bars for quantum defects $\mu = 0.2 \pm 0.1$ for carbon, and 0.12 ± 0.07 for oxygen. Transitions from states with values of $n < 5$ for carbon and $n < 6$ for oxygen are energetically forbidden.

Assuming an isotropic angular distribution of the electrons in the projectile rest frame and estimating the transmission function of the analyzer, a crude estimate of cross sections for the production of autoionizing states was made. For 25-MeV O^{4+} on Ar the total cross section for producing the state corresponding to the most intense line ($n = 6$) is $\sim 1-2 \times 10^{-19}$ cm^2. Summing over all lines up to the series limit, one gets a cross section which is about four times larger. A comparison with total-projectile electron-loss cross sections measured by Macdonald and Martin[23] shows that the fraction of electrons emitted in the autoionization channels discussed here is $\sim 1\%$ of the total electrons lost.

A comparison with Si data obtained in earlier, lower-resolution measurements strongly suggested that the structure there originates from the same kind of autoionization states. The lowest distinct structure corresponds to an energy in the projectile frame of about 4.3 eV. This energy was assigned to transitions from states with $n = 9$. In order to explain the similar structures observed with Si^{11+} (and Si^{12+}), simultaneous single capture with excitation or double capture into excited states has to be considered. In fact in all the collision processes discussed here, two-electron transition processes are required to account for production of the observed states. The one- and two-electron capture processes apparently have high cross sections at the lower beam energies (less than 2.5 MeV/u), where strong structures were found for Si^{11+} and Si^{12+} projectiles, but have much smaller cross sections at energies above 3.5 MeV/u, where they were not discernible.

Thus, the analysis of electrons emitted into the forward direction permits the study of doubly excited, high Rydberg autoionizing states where low Auger energies (2–20 eV) can be very conveniently detected. For Be-like ions, there is a high probability for simultaneous excitation of both electrons to bound states (one high lying). For silicon, double-electron-capture events to excited states of the projectile and events in which there is simultaneous capture and excitation involving the electrons were found to have high cross sections at energies below 2.5 MeV/u. The single- and double-electron-capture cross sections have comparable magnitude.

C. Forward electron ejection in ion-solid collisions: Convoy electron production

As noted in Sec. I, in contrast to ECC and ELC cusp shapes, the cusps characterizing "convoy" electron production in ion-solid collisions are skewed toward high electron velocities, but exhibit velocity-independent widths very similar to ELC widths. While the shape of the convoy peaks is independent of projectile Z and of target material, the yields in polycrystalline targets exhibit a strong dependence on projectile Z and velocity, and a weak target Z dependence.[32] Numerous attempts have been made to link convoy electron production to binary ECC or ELC processes, often at the exit surface.[32,33,29] Alternatively, a solid-state wake-riding model has been proposed.[20,34] Measured dependences[32] of shape and yield on projectile charge state and energy are inconsistent with the predictions of either theory.[9,20,34]

A key parameter for comparison of theory and experiment is the full width at half maximum Γ_l of the longitudinal velocity distribution of the electrons emerging in the forward direction. In the ECC theory of Dettmann *et al.*,[9] Γ_l can be expressed as $\Gamma_l = (\frac{3}{2}) v \theta_0$, where v is the projectile velocity in a.u. and θ_0 is half the acceptance angle, in radians, of a suitable electron velocity analyzer. For ECC in gaseous targets, experimental results are only roughly consistent with this prediction. For solid targets, some authors[17,32,35] observe Γ's that are essentially independent of the velocity of the projectile. Our results for heavy ions are at odds with the ECC prediction and any assumption that the "last target layer" is the source of the continuum electrons (if produced by ECC). The velocity distribution of continuum electrons coming from wake-riding (WR) states is predicted to be significantly different from the velocity distribution of ECC electrons. The FWHM's of the longitudinal velocity distribution for wake-riding electrons as predicted by Brandt and Ritchie[20] are shown in Fig. 6; they depend on the target material and the atomic number of the projectile and are a decreasing function of the projectile energy. Our corresponding experimental results are also shown in Fig. 6.

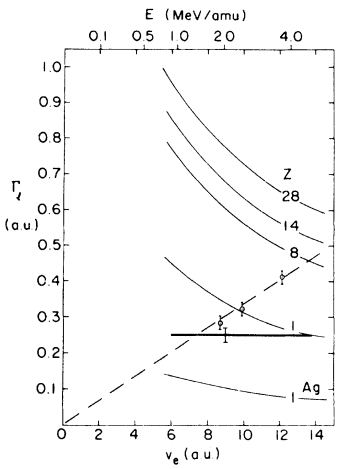

FIG. 6. The full width at half maximum of the longitudinal electron velocity distribution Γ_l, in a.u., for continuum electrons as a function of the electron velocity v_e, in a.u. The incident projectile energy, in MeV/u, appears at the top of the figure. The dashed line is the ECC prediction. The solid lines are the predictions of the WR theory for an Al target with the indicated projectiles. The lowest solid curve marked Ag is the prediction of WR theory for protons incident on Ag. The experimental data for solids correspond to $\Gamma_l \cong 0.25$ a.u. and are represented by the heavy solid line. The open points represent the gaseous targets (Ne and Ar) results for O^{8+} and Si^{14+}. From Laubert *et al.*, Ref. 35.

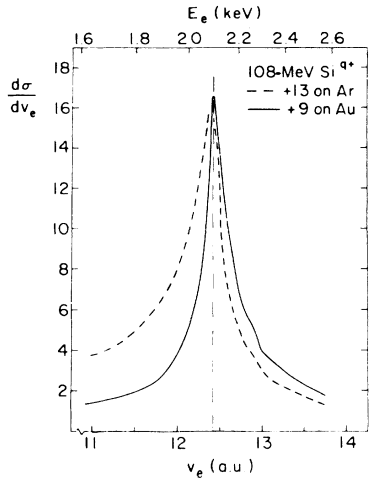

FIG. 7. The differential production cross section $d\sigma/dv_e$ as a function of the electron velocity v_e of continuum electrons emerging near 0° with respect to the ion beam, for 108-MeV Si^{13+} in Ar gas at 30 mTorr and for Si^{9+} on a 100-μg/cm^2 Au foil. The electron energy scale appears at the top of the figure. The mean emergent charge from the solid target is also 13. From Laubert *et al.*, Ref. 35.

Our past and more recent experiments with protons, oxygen, silicon, and nickel projectiles on polycrystalline C, Al, Ag, and Au targets all give a (somewhat geometry-dependent) FWHM of $\Gamma = 0.25$ a.u., but do not show the dependence on the variables (e.g., Z, v) discussed in present theories. The experimental results are clearly at variance with present theoretical predictions. Distinct differences in the cusp electron distribution are evident for solid compared to gaseous targets. A typical velocity spectrum is shown in Fig. 7 for 108-MeV Si incident on Ar (gaseous) and Au (solid) targets. For solid targets the velocity distribution is narrower and exhibits a skew toward the high velocity side. Apart from the skew, the convoy spectra are similar to ELC spectra acquired under similar conditions.

To aid in unraveling this puzzling array of similarities and differences, we have more recently initiated coincidence experiments to investigate the dependence of shape and yield of the convoy electron spectrum on the charge q_e of the associated emergent ion for ions traversing polycrystalline targets as well as for well-channeled ions traversing a gold monocrystal. For the best channeled ions, the fact that their charge often does not change throughout their entire crystal passage[36] makes such channeled ions useful probes. Discussion of these more recent results is deferred to Sec. IV.

III. EXPERIMENTAL PROCEDURES

A key feature of our experimental procedures is the easy intercahnge of short gaseous and thin solid targets at the same physical position, with all apparatus aperture sizes, dimensions, positions, and other experimental details unaltered. It has therefore been possible to cancel most systematic apparatus effects in comparing gaseous- and solid-target results. Using appreciably heavier bare and few-electron ions than heretofore under single ion-atom collision conditions and extending the velocity range and charge-state variation of measurements appreciably above those of earlier experiments, and using electron-scattered ion-coincidence techniques, we have been able to test experimental predictions of ECC and ELC theories for gases which have been inaccessible in previous experiments. The simple interchange of gas and solid targets then permits direct comparisons of spectra and yields.

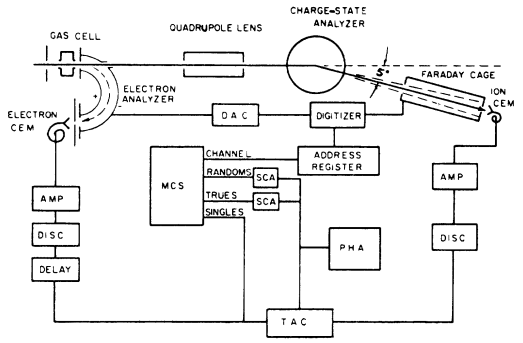

FIG. 8. Schematic diagram of electrostatic version of the experimental apparatus, showing coincidence arrangement used.

Schematic diagrams of suitable apparatus are displayed in Figs. 8 and 9. Projectile ions from the Oak Ridge National Laboratory Tandem, Brookhaven National Laboratory Tandem, Lawrence Berkeley Laboratory Super-HILAC, or other accelerators traverse thin gaseous or solid targets over a velocity range corresponding to 0.7—8.5 MeV/u. Beams are typically collimated to $\frac{1}{3}$-mm diameter and $\pm 0.025°$ angular spread, and then traverse a 4-mm thick target cell terminated by $\sim$2-mm apertures (or a foil target centered at the same location). In the case of Fig. 8, the beam and accompanying electrons then enter along the central ray of a 180° spherical-sector analyzer of mean radius 3.8 cm, whose $\Delta E/E$ of 1.4% full width at half maximum is set by a 0.71-mm analyzer exit aperture and the beam diameter at the center of the cell. Typical gas pressures of $\sim$15 mTorr are established by a standard feedback-controlled capacitance-manometer system. Single-collision conditions and negligible charge changing are verified by checking linearity plots of integrated cusp cross sections versus pressure for the various incident ions and energies. The plot intercepts typically coincide with low-residual cusp-production cross sections measured at zero pressure. Spurious signals from electron loss by contaminant beams can be ruled out, as deliberate changes in the accelerator vacuum by a decade in pressure produced no noticeable effect on pressure linearity. The collimation of the ion beam guarantees that the beam never encounters any aperture or surface in the gas cell or spectrometer regions, as verified by the low spurious signals obtained at zero pressure. Magnetic fields are reduced to $<3\times10^{-6}$ T over the spectrometer volume by three orthogonal external coils. Changes in coil current of $\lesssim 20\%$ produce negligible changes in cusp shape and integrated production cross sections.

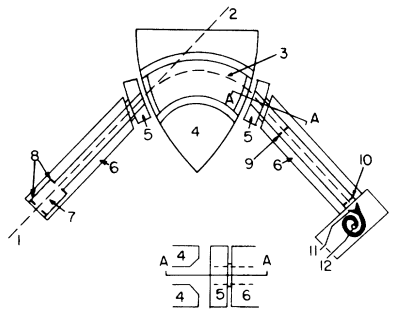

FIG. 9. Schematic diagram of magnetic sector spectrometer. Ion beam enters spectrometer (1) and exits to Faraday cup (or CEM) (2). Electrons from curved path (3) through pole pieces (4). Mirror pieces (5) shape field edges for improved focusing. Shield pieces (6) minimize magnetic fields along electron path, house gas cell (7) defined by apertures (8), angle-defining aperture (9), and exit aperture (10). Channel electron multiplier (CEM) (12) detector has negatively biased cone (11).

The ion beam passes through an opening in the larger radius sector of the electron-energy analyzer and is subsequently focused by a magnetic quadrupole doublet, and dispersed horizontally according to its charge state by a perpendicular magnetic field. One selected charge state is collected by a channel electron multiplier located approximately 6 m from the target, while the other charge states are collected in a Faraday cup. This arrangement allows us to determine the charge state of the emergent ion and permits beam normalization. It also permits the detection of energy-analyzed electrons in coincidence with emergent ion of a selected charge state. The start signal for a time-to-amplitude converter (TAC) is generated by the detection of a energy-analyzed electron, while the stop signal is generated by the detection of a charge-analyzed ion. The resultant TAC distribution has a peak of full width at half maximum of $\sim$6 nsec, which indicates a coincidence event between the detected electron and charge-analyzed particle. In a similar manner the number of accidental events is counted. The total particle flux is adjusted so that the true-to-accidental ratio is typically 100-to-1 but is always constrained to exceed 5-to-1 by beam flux adjustment. This experimental arrangement allows us to measure the number and energy distribution of all the emitted electrons (i.e., the "singles" spectrum), the number

and energy distribution of electrons (corrected for accidental events) detected in coincidence with a particular charge state of the emergent ion (coincidence spectrum), the total number of ions of a certain charge state, and the total number of ions.

Figure 9 shows a magnetic variant appropriate to use with projectiles above the Coulomb barrier. Using such experimental arrangements we have employed bare, one- and multi-electron projectile ions on He, Ne, and Ar targets (under single-collision conditions); equilibrium thickness self-supporting polycrystalline C, Al, Ag, and Au targets; and monocrystalline Au targets oriented for axial channeling (⟨110⟩ and ⟨100⟩) and random directions. Since there are several distinct aspects to the more recent experimental results, we discuss them separately and comparatively.

IV. RECENT EXPERIMENTAL RESULTS

A. ECC singles measurements

From our data we extract absolute values for the differential cross section $d\sigma/d\Omega$ for ECC by numerically integrating the cusp-shaped velocity distribution over the velocity interval $v(1\pm\alpha)$. We define the differential cross section for electron ejection into a small cone of half angle θ_0 about the forward direction by

$$\left.\frac{d\sigma}{d\Omega}\right|_{\alpha}^{\Delta\Omega(\theta_0)} = \frac{1}{\Delta\Omega}\int_{\Delta\Omega(\theta_0)}\int_{v(1\pm\alpha)}\frac{d^2\sigma}{d\Omega\, dv_e}\,dv_e\,d\Omega\ . \tag{8}$$

This cross section obviously depends on the integration limits, i.e., on α. If the angular distribution of ECC electrons is cusp shaped about the forward direction, then $(d\sigma/d\Omega)|_{\alpha}^{\Delta\Omega(\theta_0)}$ also depends strongly on the acceptance angle θ_0 of the electron-energy analyzer and increases as θ_0 is decreased. When comparing results obtained with different experimental setups, care must be taken that the integration limits and the chosen solid angle $\Delta\Omega$ are noted.

Absolute values for the cross sections are obtained from the raw data of electron counts/channel using the following equations:

$$\left.\frac{d\sigma}{d\Omega}\right|_{\alpha}^{\Delta\Omega(\theta_0)} = Y_\alpha C\ , \tag{9}$$

where

$$Y_\alpha = \sum_j N_j(v_{e_j})\Delta v_{e_j}\left[\frac{Z}{QP}\right], \qquad v_{e_j}=v(1\pm\alpha)$$

$$C=\frac{2\times(1.6\times10^{-10})}{3.23\times10^{13}}\frac{1}{\beta T_{\rm eff}(v)\Delta x\,\Delta\Omega}\ . \tag{10}$$

Here $N_j(v_{e_j})$ is the number of electrons counted in the jth channel, Q is the charge collected in the Faraday cup during one channel of data collection in nC, and P is the target gas pressure in mTorr. The energy resolution $\Delta E/E$ (FWHM) of the electron-energy analyzer is denoted by β and a triangular analyzer function is assumed. $T_{\rm eff}(v)$ denotes the transmission/detection efficiency of the detector at electron velocities near the ion velocity and Δx denotes the target thickness.

The relative yields Y_α are obtained from the raw data. Instead of measuring each of the parameters β, $T_{\rm eff}(v)$, Δx, and $\Delta\Omega$ independently, the factor C has been determined at one ion velocity by measuring the yield for processes where the absolute cross section is also known. Our absolute values for $(d\sigma/d\Omega)|_{\alpha}^{\Delta\Omega(\theta_0)}$ have been normalized to published cross sections for Ar-L-Auger emission by Stolterfoht *et al.*[24] as noted above.

The uncertainties in the absolute values of $(d\sigma/d\Omega)|_{\alpha}^{\Delta\Omega(\theta_0)}$ are estimated to be $\sim\pm40\%$, the major sources being the uncertainty in the absolute cross section by which the instrument was calibrated ($\sim20\%$), the uncertainty in the background corrections for Ar L-Auger yield measurements ($\sim10\%$), and uncertainties in the relative efficiency of the instrument ($\sim10\%$).

In Sec. II we have compared absolute values of the cross section $d\sigma/d\Omega$ obtained from our data with results of Rødbro and Andersen[11] (Fig. 3), who subtracted a fitted background from their cusps. To make valid comparisons of the two results it was necessary to subtract a similar background from our data. However, as has been noted in Sec. II, no unambiguous subtraction of the direct ionization component in the region of the ECC cusps is possible. In Table I we therefore present our results with and without background subtraction together with Rødbro and Andersen's results. To evaluate background-subtracted cross sections, we integrate the entire cusp above the background. The cross sections which include the background were integrated over the limits $v(1\pm\alpha)$, $\alpha=0.04$. Therefore, the background-subtracted cross sections are larger than the ones including background. A second comparable set of

TABLE I. Absolute cross sections for ECC from H^+ and D^+—Ne and Ar.

Projectile ion	Energy (MeV/u)	Velocity (a.u.)	Target	$\left[\frac{d\sigma}{d\Omega}\right]^a$	$\left[\frac{d\sigma}{d\Omega}\right]^b$	$\left[\frac{d\sigma}{d\Omega}\right]^c$	$\left[\frac{d\sigma}{d\Omega}\right]^d$
				$\times(10^{-19}$ cm^2/sr)			
D^+	0.70	5.29	Ar	22.8	20.3	16.9	12.0(H^+)
D^+	0.70	5.29	Ne	25.2	25.0	18.0	16.0(H^+)
H^+	1.40	7.49	Ar	5.8	5.0	7.0	
H^+	1.88	8.70	Ar	1.7	1.8		
H^+	2.00	8.94	Ar	1.3	1.3	3.1	

[a]Present measurement with yield integral and background subtraction identical to that of Ref. 11, $\theta_0 = 1.8°$.
[b]Source: Rødbro and Andersen, Ref. 11 (1.88- and 2.0-MeV/u points extrapolated from 1.7 Mev/u). Integrating the entire cusp above background, $\theta_0 = 0.36°$.
[c]Present measurement integrating over limits $v(1+\alpha)$, $\alpha = 0.04$; no background subtraction, $\theta_0 = 1.8°$.
[d]Source: Cranage and Lucas, Ref. 14; no background subtraction, $\theta_0 = 2.86°$.

absolute cross-section data for ECC processes is that of Cranage and Lucas[14] for 300—1200 keV protons traversing H_2, He, Ne, and Ar targets. Their cusps were integrated over the constant velocity interval $(v \pm v_B/4)$, where v_B is the first Bohr orbit electron velocity. Their acceptance angle θ_0 was 0.05 rad. Their results without subtraction of large, slowly varying backgrounds, are compared to ours in Table I. Differences of about $\pm 10\%$ are expected solely because of the different limits of integration used.

The integration limits $v(1 \pm \alpha)$ were chosen after carefully examining the shape of the velocity distribution of the ECC electrons. In order to provide some parametric measure of the shape as a function of ion velocity v, ion charge Z, and target gas, the half-widths at half maxima for both the low-energy and the high-energy side of the cusp-shaped peaks have been measured and corrected for analyzer-dependent errors. Due to the finite energy resolution $\Delta E/E$ of our electrostatic energy analyzer, the full widths at half maxima are systematically in error because of errors in the observed height of the peak. In addition, the widths of the cusps are expanded from convolution with the analyzer function.[18,19]

The following procedure was followed in correcting Γ_L and Γ_R from our ECC data. The observed Γ_L were reduced by 10% to correct for peak height distortion, while the observed Γ_R were reduced by 20% to correct for the convolution broadening of the narrow widths. This procedure is consistent with corrected widths found from deconvolution of measured analyzer functions from observed ECC peaks.

Results are displayed in Table II and Figs. 10 and 11 for O^{8+} and Si^{14+}, respectively, traversing He, Ne, and Ar.

The half-widths of the high-energy side, Γ_R, are narrower than predicted by the analytic form of Dettmann *et al.*[9] and are observed to be target, projectile Z, and nearly projectile-velocity independent over the ranges measured. The small-v dependence is fully consistent with the increase expected from the analyzer resolution alone.

The low-energy side half-widths, Γ_L, are wider for all cases than the corresponding Γ_R, in contradiction to predicted symmetric peak shapes in the theory of Dettmann *et al.*[9] It is noted, however, that the He and Ar cusp half-widths, Γ_L, do vary approximately linearly with ion velocity throughout the full range $v = 8 - 12.5$ a.u. as predicted, while the half-width, Γ_L, for Ne target *does not.* The increase in Γ_L from 0.29 to 0.49 a.u. in the interval $v = 8.7 - 10$ a.u. has been reexamined in greater detail with a 30° parallel-plate electrostatic analyzer of higher intrinsic energy and angular resolution than the spherical-sector analyzer employed for the bulk of this study. The results are displayed in Fig. 12 where a sharp rise in Γ_L is noted at $v \cong 10$ a.u.

The increase in Γ_L occurs when the projectile velocity nearly matches the Ne K-shell electron-orbital velocity. Similarly for 15- and 18.1-a.u. Ar^{18+} projectiles on He, Ne, and Ar targets, the low-energy side half-width Γ_L increases approximately linearly with v for He and Ne but rises more steeply for Ar targets, where for 18.1-a.u.

TABLE II. Half-widths at half maxima measured for ECC cusps.

Projectile ion	Energy (MeV/u)	Velocity (a.u.)	Target	Γ_L (a.u.)	Γ_R (a.u.)
O^{8+}	30	8.70	Ar	0.28	0.06
O^{8+}	30	8.70	Ne	0.32	0.07
O^{8+}	30	8.70	He	0.18	0.06
O^{8+}	40	10.04	Ar	0.29	0.07
O^{8+}	40	10.04	Ne	0.55	0.06
O^{8+}	40	10.04	He	0.22	0.08
O^{8+}	51	11.34	Ar	0.37	0.09
O^{8+}	51	11.34	Ne	0.56	0.08
O^{8+}	51	11.34	He	0.24	0.08
O^{8+}	61.8	12.48	Ar	0.41	0.08
O^{8+}	61.8	12.48	Ne	0.63	0.06
O^{8+}	61.8	12.48	He	0.2 ± 0.1	0.1 ± 0.05
Si^{14+}	70	10.04	Ar	0.30	0.10
Si^{14+}	70	10.04	Ne	0.41	0.06
Si^{14+}	90	11.39	Ar	0.32	0.10
Si^{14+}	90	11.39	Ne	0.47	0.08
Si^{14+}	90	11.39	He	0.4 ± 0.2	0.1 ± 0.1
Si^{14+}	108	12.47	Ar	0.36	0.06
Si^{14+}	108	12.47	Ne	0.54	0.06

projectiles the ion velocity exceed the Ar K-shell electron-orbital velocity.

Therefore, ECC peak shapes are found to be highly target dependent even approaching $v_e = v$ for ion velocities near the target electron-orbital velocities. However, comparing cusp shapes for different projectiles but the same targets reveals little or no Z dependence in the shape.

In order to determine the velocity and Z dependence of the ECC cross section we have to assure that we integrate over a constant fraction of the cusp. Since apart from target-shell effects the low-energy side half-width and the full width at half maximum increase linearly with v, the integration limits $v(1\pm\alpha)$ satisfy this criterion.

In Table III we present absolute values of the differential cross section $(d\sigma/d\Omega)\,|_{\alpha=0.04}^{\Delta\Omega(1.8^\circ)}$ for ECC for 1.8–3.9-MeV/u C^{6+}, O^{8+}, and Si^{14+} on He, Ne, and Ar. The cross sections are plotted versus ion velocity in Figs. 13, 14, and 15. For the

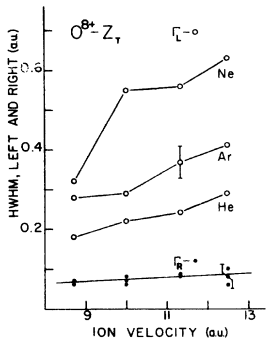

FIG. 10. Half-widths at half maxima on lower, Γ_L, and higher, Γ_R, energy sides of the forward ECC peaks for O^{8+}-Ar, -Ne, and -He.

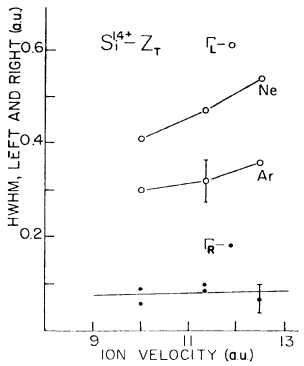

FIG. 11. Half-widths at half maxima on lower, Γ_L, and higher, Γ_R, energy sides of the forward ECC peaks for Si^{14+}-Ar and -Ne.

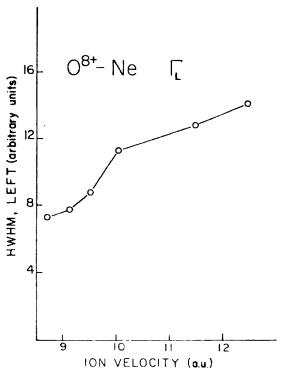

FIG. 12. Half-widths at half maxima on lower-energy side of the forward O^{8+}-Ne ECC peaks.

same targets, curves for different projectile ions are nearly linear and parallel, depicting both a common velocity dependence and a velocity-independent Z dependence.

For the O^{8+}-Ar and -He data the velocity dependences are found, through computer fitting of the data, to be well represented in this energy region by $v^{-4.3\pm0.3}$ and $v^{-8.4\pm0.6}$, respectively, but that for O^{8+}-Ne is less well represented by any simple power law. It is interesting to note that the approximate velocity dependence of the *total* cross sections for single-electron capture for O^{8+}-He and -Ar are approximately the same as these. MacDonald and Martin[23] find for O^{8+} velocities greater than $\sim$4.5-a.u. total single-capture dependences of $\sim v^{-3}$ for Ar and $\sim v^{-8}$ for He.

While the conditions for validity of the Born approximation are incompletely met for these many-electron targets, where only inner-shell electrons may have orbital velocities in excess of the projectile velocity, a comparison with the predicted velocity dependence is revealing. The first Born theory of Dettmann *et al.*[9] yields a nearly target-

TABLE III. ECC cross sections—no background subtraction.

Projectile ion	Energy (MeV/u)	Velocity (a.u.)	Target	$\left[\frac{d\sigma}{d\Omega}\right]\Big\|_{\alpha=0.04}^{\Delta\Omega(1.8°)}$ $\times(10^{-19}$ cm^2/sr)
C^{6+}	1.88	8.70	Ar	179.0 ± 63.0
C^{6+}	1.88	8.70	Ne	76.9 ± 27.0
C^{6+}	1.88	8.70	He	4.95± 1.7
C^{6+}	2.50	10.04	Ar	96.0 ± 34.0
C^{6+}	2.50	10.04	Ne	35.5 ± 13.0
C^{6+}	2.50	10.04	He	1.29± 0.90
C^{6+}	2.75	10.55	Ar	83.1 ± 29.0
O^{8+}	1.60	8.03	Ar	432.0 ±151.0
O^{8+}	1.88	8.70	Ar	353.0 ±124.0
O^{8+}	1.88	8.70	Ne	149.0 ± 52.0
O^{8+}	1.88	8.70	He	8.03± 2.8
O^{8+}	2.25	9.53	Ar	237.0 ± 83.0
O^{8+}	2.50	10.04	Ar	182.0 ± 64.0
O^{8+}	2.50	10.04	Ne	101.0 ± 35.0
O^{8+}	2.50	10.04	He	3.1 ± 1.1
O^{8+}	3.25	11.34	Ar	108.0 ± 38.0
O^{8+}	3.25	11.34	Ne	37.8 ± 13.0
O^{8+}	3.25	11.34	He	0.93± 0.65
O^{8+}	3.86	12.48	Ar	64.8 ± 23.0
O^{8+}	3.86	12.48	Ne	24.6 ± 8.6
O^{8+}	3.86	12.48	He	0.44± 0.31
Si^{14+}	2.50	10.04	Ar	637.0 ±223.0
Si^{14+}	2.50	10.04	Ne	238.0 ± 83.0
Si^{14+}	3.21	11.39	Ar	350.0 ±123.0
Si^{14+}	3.21	11.39	Ne	104.0 ± 36.0
Si^{14+}	3.21	11.39	He	4.3 ± 1.5
Si^{14+}	3.86	12.47	Ar	250.0 ± 87.0
Si^{14+}	3.86	12.47	Ne	85.0 ± 30.0

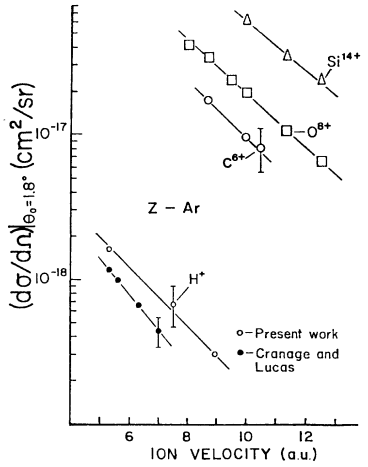

FIG. 13. ECC singly differential cross sections for H^+, C^{6+}, O^{8+}, and Si^{14+} on Ar. Velocity integration interval is $v(1-\alpha)$ to $v(1+\alpha)$, $\alpha = 0.04$. Comparison is made to the work of Cranage and Lucas (Ref. 14).

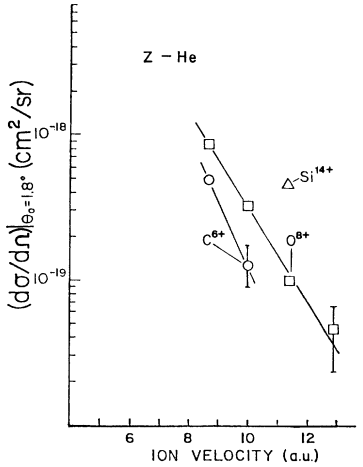

FIG. 15. ECC singly differential cross sections for C^{6+}, O^{8+}, and Si^{14+} on He. Velocity integration interval is $v(1-\alpha)$ to $v(1+\alpha)$, $\alpha = 0.04$.

independent approximate v^{-10} power law for total ECC cross sections, while Macek's[5] treatment with scaled hydrogenic target wave functions gives a $v^{-9.2}$ dependence for He targets.[11] The Ne and Ar target data obtained here have experimental velocity dependences significantly different from v^{-10}, but the He target velocity dependence is much nearer the theoretical values. This might be expected since the He electron velocity is less than one-sixth that of the 8.7-a.u. projectiles for example, and only 1*s* electrons can contribute, as is assumed in the development of the theories. However, Z_T/v, the parameter usually considered important in determining the applicability of the Born approximation, is equal to 1 for the 8.7-a.u. velocity-projectile case, in clear violation of the assumption that it is much less than 1.

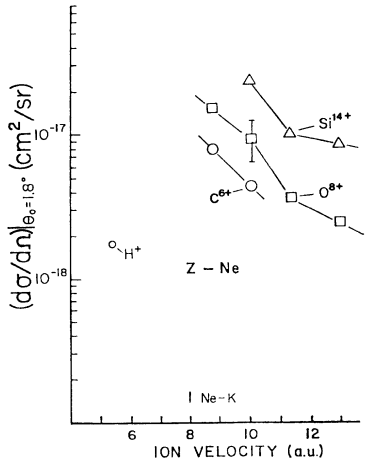

FIG. 14. ECC singly differential cross sections for H^+, C^{6+}, O^{8+}, and Si^{14+} on Ne. Velocity integration interval is $v(1-\alpha)$ to $v(1+\alpha)$, $\alpha = 0.04$.

For the O^{8+}-Ne data displayed in Fig. 14 there is an observable deviation from strict power-law dependence in the region between 9–10 a.u. It is assumed that this increased yield originates from Ne *K*-shell capture to the continuum and is a phenomena related to velocity matching of the projectile and target electrons, since the Ne *K*-shell orbital velocity is approximately 8 a.u. as labeled in Fig. 14. The increased yield arises because of a rapid rise in the low-energy side of the peak at ion velocities beyond $v = 8$ a.u.

It is also suspected that the slow velocity variation for Ar target data in the velocity region studied is in part due to the increased Ar *L*-shell contribution to continuum capture, which shows an onset at about $v \cong 6$ a.u.[11] The same onset or additional contribution is observed in O^{8+}-Ar *total* electron-capture cross sections but at a slightly higher incident ion velocity.

Since the velocity dependences of the observed cross sections are target specific, there is no unique Z_T power scaling, as predicted by the theory due Dettmann *et al.*,[9] where Z_T^5 is calculated. A forced power-law fit to the data for O^{8+} at $v = 10.04$ a.u. gives $Z_T^{1.8\pm0.6}$.

A significant prediction of the theory of Dettmann *et al.*,[9] and also that due to Macek,[5] is a Z^3 dependence for the cross section, which is almost independent of ion velocity.

The *Z* dependence of our data is graphically

displayed in Fig. 16, where it is seen that a simple power law satisfactorily describes the Z-Ar data at 2.5 MeV/u for all projectiles. The point for $Z=1$ on this graph is taken from an extrapolation of the H^+-Ar data in Fig. 16 to 2.5 MeV/u, hence the relatively large uncertainty displayed in the figure for that data point. Representing the cross sections as proportional to Z^p, with p determined through a least-squares fitting of the data, gives $p=2.3\pm0.3$. Variation of the limits of integration from $\alpha=0.01$ to 0.04 has shown no tendency to resolve the disagreement. Similarly, yields calculated for ECC peaks from O^{8+} and Si^{14+} traversing argon target gas, and from which direct ionization backgrounds have been subtracted, exhibit the same $\sim Z^{2.3}$ dependence.

The theories of Macek and Dettmann *et al.*, discussed in Sec. II predict a symmetric peak in the velocity distribution of ECC electrons emitted into a small cone about the forward direction. A potentially important step forward was made recently by Shakeshaft and Spruch.[1] They suggested that the asymmetry of all measured ECC cusps might be the first experimental indication of the importance of including the second Born term in Born expansion calculations, even though the impact velocities were appreciably below that required to assure dominance in total cross section. In the first Born approximation the shape of the cusplike peak observed in the ECC velocity distribution is centered at $v_e=v$ and is symmetric about v, owing to a $\sim v^{-2l}$ dependence for ejected-electron partial

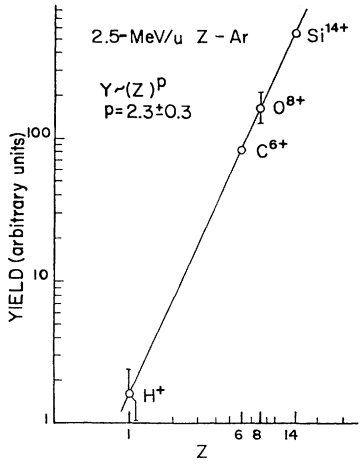

FIG. 16. Z dependence of singly differential cross section for 2.50-MeV/u Z-Ar.

waves. However, for the second Born term all partial waves are thought to have comparable importance. The first Born term depends only on the magnitude of the vector $(\vec{v}_e-\vec{v})$, implying an isotropic velocity distribution in the rest frame of the projectile characteristic of s-wave continuum states. Theoretically the asymmetry arises entirely from second Born terms for which the differential cross section $d\sigma/dv_e$ is asymmetric under the transformation $(\vec{v}_e-\vec{v}) \Longrightarrow -(\vec{v}_e-\vec{v})$.

A counterconjecture concerning the origin of the observed asymmetry is provided by Chan and Eichler[37] who note that retention of terms linear in $\Delta v_e/v=(\,|\,\vec{v}_e-\vec{v}\,|\,)/v$ beyond those incorporated in the first-Born-Brinkman-Kramers (BK) approach originally used by Dettmann, Harrison, and Lucas produces a similar asymmetry. However, predictions of Refs. 1 and 37 concerning the projectile Z and v dependence of both shape and yield are very different, as is the predicted shape of the corresponding cusps.

The characteristic feature of the Shakeshaft and Spruch (SS) shape is the sheer drop on the high-velocity side of the peak. When convoluted with the instrument function, a drop is expected whose slope and width are essentially determined by the analyzer resolution function. This property is not shared by the Chan and Eichler (CE) shape. Furthermore, the CE shape is predicted to become symmetric at high v as $\sim 1/v$. To test both conjectures we measured ECC spectra for higher velocities (15–18 a.u.) and for heavier bare projectiles (Ar^{18+}) than ever used heretofore in He, Ne, and Ar. The ECC asymptotic velocity dependence of $d\sigma/dv$ predicted by Dettmann, Harrison, and Lucas,[9] when integrated over an appropriately scaled velocity region [e.g., $(1-\alpha)v$ to $(1+\alpha)v$ with $\alpha=0.04$] is v^{-10}. The dependence coincides with our experimental results for Ar^{18+} in He, which (over the range $v=15-18$ a.u.) scale as $\sim v^{9.9}$, suggesting that the asymtotic velocity region has been reached (not so for either Ne or Ar targets, where the yields scale as v^{-7} over the same range).

The magnetic-sector electron spectrometer was used in this experiment with an acceptance cone of half angle $\theta_0=1.7°$ centered on the forward direction and a momentum resolution of 1.7% (FWHM).

Typical data for Ar^{18+} on He are displayed in Fig. 17 overlaid with the best fits to the data obtained with a convoluted Shakeshaft-Spruch line shape (curve a) and a convoluted Chan-Eichler line shape (curve d). Data were acquired over a wider

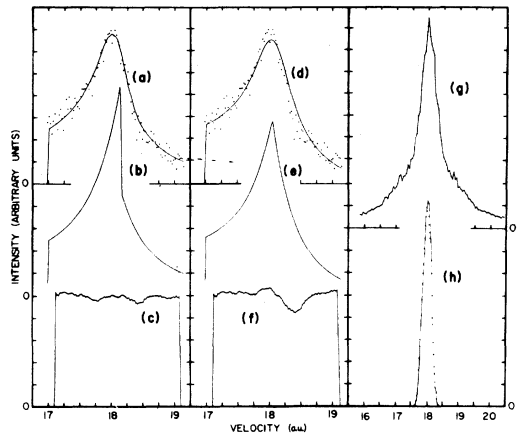

FIG. 17. Comparison of the central portion of ECC cusps obtained for 18.1-a.u. Ar^{18+} on He with the overlaid convoluted line shapes read from Ref. 1 (a) and Ref. 37 (d). The respective best-fit theoretical shapes (b) and (e), when convoluted with the measured apparatus function (curve h), produce fits (a) and (d). A narrower more symmetric ELC spectrum for 8.5-MeV/u Ar^{13+} on He is shown in (g). Curves (c) and (f) display ten channel moving averages of the corresponding deviation spectra ($y_i - y_{\text{fit}}$ vs i) as discussed in the text.

velocity range, but since detailed line-shape predictions apply only very near $v = v_e$, only the corresponding region is displayed. Convolution of parametrized theoretical line shapes (curves b and e) with the 1.7% FWHM measured apparatus function shown in curve h (from-electron-gun calibration data) yielded the best fits (curves a and d). That the asymmetries observed are valid is demonstrated in curve g, which depicts the narrower, much more symmetric line shape (with Auger structure superposed) obtained for forward electron loss from 8.5-MeV/u Ar^{13+} on He. Here only the incident beam was switched, with all other conditions unaltered.

Because the theoretical curves b and e apply to $Z = 6$ at 9 a.u. in a hydrogenic target, our comparisons are only partially appropriate. However, they indicate that a calculation for $v = 15-20$ a.u. in He would be very worthwhile.

Standard reduced X^2 tests, in addition to a deviation test to be described, exhibit a marked preference for the SS as opposed to the CE shapes. For the data of Fig. 17 the fitted SS line shape yields $X^2 = 1.2 \pm 0.2$, whereas the CE shape yields 1.8 ± 0.4. At the same velocity, the analogous values are $X^2 = 6.5$ and 10 for Ne, and 8.9 and 10.8 for Ar. These values demonstrate the inappropriateness of a single-cusp fit to data we expect to be characterized by overlapping a cusp of a somewhat different width for each target shell. Curves c and f are derived from the deviation spectrum ($y_i - y_{\text{fit}}$ vs i) corresponding to a and b. To extract trends from the large statistical scatter in the deviation spectrum, we have used a moving-average technique. Curves c and f represent ten-channel moving averages, smaller than but of the same order as the analyzer resolution (16 channels). The clear preference for the SS versus the CE fit is exhibited by the large dip in curve f, which shows that the CE shape simply lacks the dropoff characterizing both the SS line shape and—by this test—the data. A moving average over fewer channels enhances the valley in the deviation spectrum (at the expense of scatter). In dozens of spectra acquired for He, Ne, and Ar, pronounced valleys were invariably observed for CE fits, and were not observed for SS fits.

A direct experimental measure of the symmetry is the ratio Γ_L/Γ_R, where Γ_L and Γ_R are the half-widths (half-maximum) of the cusp to the left and right of the peak. At 15 a.u. the measured values in He, Ne, and Ar are 1.78, 2.64, and 2.08, respectively. At 18 a.u. they are 2.08, 2.28, and 2.57, respectively. The range errors are $\sim \pm 0.3$ in each case.

Though the present shape and velocity-dependence data are much better in accord with Ref. 1 than with Ref. 37, other predictions of Ref. 1 are not observed. For example, the asymmetries observed in Ne and Ar are very similar for all bare projectiles for Z in the range $6-18$, a finding not in accord with a predicted strongly Z-dependent asymmetry. Also, the yields scale at $\sim 1{:}200{:}500$ for 18-a.u. Ar^{18+} on He, Ne, and Ar, respectively, a dependence much weaker than a simple Z_T^5 dependence. Here, the theoretical restriction to the case of asymptotic velocities in hydrogen may be limiting.

More recently Lucas *et al.*[38] have given a simple physical interpretation of the step-function behavior of the cusp displayed in Fig. 17, showing that it directly indicates the relative importance of higher waves, and Macek *et al.*[39] have extended the discussion of Shakeshaft and Spruch[1] to consider other evidence for second Born term contributions to the ECC cross sections. Meckbach *et al.*[40] have independently discussed higher partial wave contributions to asymmetries, which they are able to characterize in a general case independent of a specific approximation.

B. ECC coincidence measurements

Similarities in the velocity dependences of ECC cross sections and cross section for single-electron capture by O^{8+} on Ar and Ne suggest a close connection between continuum- and bound-state capture. We have initiated coincidence experiments where we measure ECC events that occur in coincidence with b bound-state-capture events ($b=0$, 1, 2, 3) for 20 and 30-MeV O^{8+} and O^{7+} on Ar. It is therefore possible to investigate the importance of simultaneous bound- and continuum-state capture. For 20-MeV O^{8+} ions undergoing single collisions in Ar gas targets, we find that additional bound-state capture of one, two, or three electrons are observed in $\sim 34\%$, $\sim 14\%$, and $\sim 3\%$ of the collisions, respectively. For 30-MeV O^{8+} on Ar, one or two additional bound-state captures occur in $\sim 32\%$ and $\sim 9\%$ of the collisions generating an ECC electron. All yields of electrons detected in coincidence with a final ion charge state are consistently normalized to the total ECC yields independent of final ion charge state. The number of b ($b=0$, 1, 2, 3) bound-state captures per 100 ECC events differ from percentages published earlier,[41] where for $b=0$ the yields were normalized to the total number of O^{8+} ions counted in the ion CEM, while for $b\neq 0$ the yields were normalized to the Faraday cup current. As the detection efficiency was somewhat different for these two detection modes, the percentages reported in Ref. 41 have been modified accordingly. While the change is not negligible, it is modest, and none of the conclusions of Ref. 41 are changed thereby. The above observations indicate a high degree of association between the processes of multiple-electron capture into bound and continuum states at the velocities used. Since our results directly demonstrate that often one or more closely associated additional bound-state captures occur whenever a continuum-capture event is observed, it is natural to raise the question, what fraction of the time does one or more continuum-state captures occur when a bound-state capture occurs? Though this question is not directly answered in the present generation of experiments because of counting-rate limitation in the ion-counting coincidence channel, we can answer this question indirectly by comparing the total cross section for coincident continuum and bound-electron capture with total cross sections measured by other authors for what has always tacitly been assumed by them to represent bound-state captures alone.

The remarkable finding is that we can consistently account for a significant fraction of what have traditionally been termed one-, two-, and three-electron bound-state-capture cross sections in terms of two-, three-, and four-electron capture events instead, where an unobserved electron has been ignored. The immediate consequence is that such comparisons as are made with bound-state-capture theories are thus being made with the wrong theories. Comparisons must instead be made with theories which explicitly include the correlated continuum-capture contributions. In Table IV data concerning the dependence of the ECC cross sections on the scattered-ion charge state are presented for 20- and 30-MeV O^{8+} and O^{7+} on Ar. These data are compared with single- and multiple-bound-state-capture data obtained by Macdonald and Martin[23] for the same collision systems at overlapping velocities. In this energy range the dependence of the cross section on beam energy for ECC coincident with $b=1$, 2, 3 bound-

TABLE IV. Cross sections for ECC acompanied by bound-state capture.

Projectile	Number of bound-state captures	20-MeV ECC cross section[b]	20-MeV Bound-state capture cross sections[a]	20-MeV Ratio	30-MeV ECC cross section[b]	30-MeV Bound-state capture cross sections[a]	30-MeV Ratio
				$\times 10^{-3}$			$\times 10^{-3}$
O^{8+}	0	5.7×10^{-20}			4.0×10^{-20}		
	1	3.9×10^{-20}	2.2×10^{-17}	1.8	2.2×10^{-20}	1.5×10^{-17}	1.5
	2	1.6×10^{-20}	6.0×10^{-18}	2.6	6.3×10^{-21}	3.6×10^{-18}	1.8
	3	4.0×10^{-21}	8.5×10^{-19}	4.7		3.8×10^{-19}	
O^{7+}	0	6.0×10^{-20}			4.7×10^{-20}		
	1	3.3×10^{-20}	1.5×10^{-17}	2.2	1.6×10^{-20}	1.0×10^{-17}	1.6

[a]From Ref. 23.

[b]Integrated over $\Delta\Omega=3\times 10^{-3}$ sr, and $v(1\pm\alpha)$, $\alpha=0.04$.

state captures are qualitatively similar to those observed in Ref. 23 for $b=1$, 2, 3, bound-state captures (ECC ignored).

C. ELC singles and coincidence measurements

In the laboratory-frame, projectile electrons that are ionized to continuum states of low momentum with respect to the projectile nucleus emerge near the forward direction and exhibit a cusp-shaped velocity distribution centered at $v_e=v$. We have systematically investigated ELC cusp shapes and yields by measuring both singles and coincidence spectra of ELC electrons. In our singles experiments cusp shapes were investigated for Si^{q+} ($q=6-14$), O^{q+} ($q=3-8$), and C^{q+} ($q=2,3$) beams with velocity 7—12.5 a.u. traversing Ar, Ne, and He targets as a function of projectile velocity v, projectile charge q, and target gas.[42] We detected electrons emitted into a cone of half angle $\theta_0=1.8°$ about the forward direction. For singles experiments we expect that the cross sections for ELC to greatly exceed the ECC cross sections whenever loosely bound projectile electrons are present. Therefore, for projectiles carrying $2p$ electrons into the collision, the measured cusps are ELC cusps. In our experiments the incident ion speed v is always greater than the intial orbital speed v_0 of the electrons to be ionized. In the limit $v>>v_0$, Briggs and Dreeper[27] predict the FWHM of ELC cusps to scale as $\frac{3}{2}v\theta_0$ similar to the cusp width for ECC. We have measured the left width at half maximum Γ_L, right width at half maximum Γ_R, and full width at half maximum Γ for each of the above ELC cusps. The widths are read directly from the measured spectra after correction for the velocity dependence of the finite-acceptance band ΔE of the analyzer. No extraneous background needs to be subtracted from any of our ELC cusp data, since signal-to-total-background ratios are high. Each measured cusp is a convolution of the "true" cusp with the analyzer function and therefore all apparent widths are expanded. The FWHM of the analyzer function, however, was always maintained below 20% of the FWHM of the measured cusp. When sufficiently intense, autoionization lines in the wings of some cusps are found to increase the apparent FWHM of the observed cusps.[30]

In Fig. 18 we plot Γ and the ratio Γ_L/Γ_R (a measure of the asymmetry) for cusps produced by 70-MeV Si^{q+} ($q=6-14$) traversing Ar and Ne.

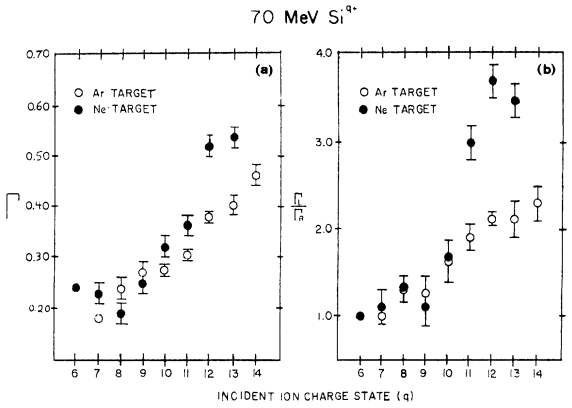

FIG. 18. (a) Full width at half maximum, Γ, and (b) the ratio of left width to right width at half maximum, Γ_L/Γ_R, of the forward electron peak for 70-MeV Si^{q+} ($q=6-14$) traversing Ar and Ne as a function of incident ion charge q. When the ECC cross section dominates the ELC cross section ($q\geq 10$) the Ne cusps become wider and more asymmetric than the Ar cusps since for Ne targets the beam velocity exceeds the K-shell electron velocity (velocity-matching criterion). Data points without error bars represent only one measurement.

We note wide and asymmetric cusps when ECC is an important contributing process. For example, $\Gamma(\mathrm{Ar})=0.46\pm0.02$ a.u. and $\Gamma_L/\Gamma_R(\mathrm{Ar})=2.3\pm0.2$ when $q=14$. If only tightly bound $1s$-projectile electrons are carried into the collisions ($q=13$, 12) the still wide and asymmetric cusps indicate that a large fraction of the cusp electrons correspond to ECC. When more loosely bound $2s$ projectile electrons are present ($q=11$, 10), the measured widths and asymmetries decrease, but only when the projectile ions carry some more loosely bound $2p$ electrons into the collision ($q\leq 9$) do the cusp asymmetries disappear within experimental uncertainties. We conclude that for Si^{q+} ($q=6-9$) projectiles, the ELC cross section dominates the ECC cross section, and the measured cusps are dominated by ELC. For O^{q+} ($q=4-8$), Vane *et al.*[22] showed that the integrated cusp yield rises steeply when projectile L-shell electrons are present. Plots of Γ_L/Γ_R against projectile charge state (O^{q+}, $q=3-8$) show that they become narrower and nearly symmetric whenever any projectile $2l$ electrons are present. Again we conclude that for O^{q+} ($q=3-5$) projectiles the measured cusps are dominated by ELC.

In Fig. 19 the FWHM of representative ELC cusps for Si^{9+} and O^{5+} projectiles on Ne and AR targets are plotted as a function of the ion velocity.

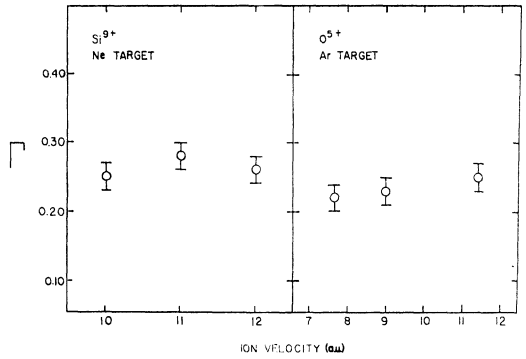

FIG. 19. Full width at half maximum, Γ, of ELC cusps as a function of ion velocity v for Si^{9+} traversing Ne, and O^{5+} traversing Ar. For Si^{q+} ($q = 6-9$), O^{q+} ($q = 3-5$), and C^{q+} ($q = 2,3$) on He, Ne, and Ar targets, Γ is found to be independent of v within experimental error.

For these projectiles, within experimental uncertainties, the FWHM of the ELC cusps are independent of projectile velocity. For Si^{q+} ($q=6-9$), O^{q+} ($q=3-5$), and C^{q+} ($q=2,3$), we have further found only a weak dependence of the FWHM on projectile charge state (mostly from broadening ing due to autoionization lines in the wings), and on the target gas (He, Ne, Ar). We summarize these results by stating that for Si, O, and C projectiles in the velocity range 7—12.5 a.u. traversing He, Ne, and Ar targets, the FWHM of the ELC cusps is $\Gamma=0.26\pm0.04$ a.u., independent of q, v, and projectile Z. Using the same experimental setup, Laubert *et al.*[35] found that the FWHM of convoy electron cusps measured when Si and O projectiles traverse solid targets (C, Al, Ag, and Au) is independent of projectile nuclear charge, projectile charge state, velocity, and target over any similar ranges, and is summarized by $\Gamma=0.25\pm0.02$ a.u., suggesting a close relationship between ELC and convoy electron-production processes. Theoretical treatments of ELC processes by Briggs and Drepper,[27] Day,[43] and Briggs and Day[44] are all approximate evaluations of the full first Born approximation of Drepper and Briggs.[26] Their conclusions should be compared with data in the region $v_0/v << 1$. Our data only marginally satisfy this criterion.

Briggs and Drepper[27] derive an expression for the doubly differential ELC cross section for a one-electron projectile on a neutral N-electron target. Since electrons ejected into a narrow cone in the forward direction are those with projectile-frame speeds $v_f \simeq 0$, the major v_f dependence in the cross section is predicted to arise from the normalization factor in a Coulomb wave centered on the projectile. Similarily, the doubly differential ECC cross section for small v_f is predicted to be primarily determined by the projectile Coulomb potential, and not by the target.

Therefore, Briggs and Drepper derive a similar analytic expression describing the cusp shape of the ELC velocity distribution as is derived by Dettmann *et al.* for ECC electrons. The FWHM of both the ELC and the ECC cusps is predicted to increase linearly with v ($\Gamma=\frac{3}{2}v\theta_0$). In the velocity range 7—12.5 a.u. we find experimentally that the FWHM of ELC cusp is nearly constant.

Day[43] and Briggs and Day[44] derive a form of the doubly differential ELC cross section in the plane-wave Born approximation, including the possibility of variations of the cross section with respect to projectile frame polar angle. The FWHM of the cusp is then given by $\Gamma=\frac{3}{2}\theta_0 v(1+\frac{3}{2}\beta+\cdots)$, $-1\leq\beta\leq2$, where the anisotropy parameter β is, in general, a function of v. The parameter β allows $\Gamma(v)$ to depart from linear behavior. However, since Γ is measured to be independent of projectile velocity, projectile nuclear charge Z, projectile charge state q, and target in the velocity range 7—12.5 a.u., severe restrictions are then placed on the velocity and Z dependences of the asymmetry parameter β.

In our coincidence experiments we again find the v, q, and projectile Z independence of the FWHM of the ELC cusps, even if the electrons are lost from 1s states. For 20-MeV O^{7+} projectiles traversing Ar the velocity spectrum of electrons detected in coincidence with a scattered O^{8+} ion is diplayed in Fig. 20 overlaid with the spectrum of all other electrons detected during the same data-taking period (normalization to the same peak height). The narrow coincidence spectrum is an ELC spectrum and has the same FWHM as all the ELC singles spectra investigated. The much broader asymmetric cusp is the spectrum of ECC electrons. A strong difference in cusp shape and FWHM is evident.

In order to compare ELC cusp yields and cross sections we have to choose consistent integration limits. Since all ELC cusps have approximately the same shape and FWHM ($\Gamma=-0.26\pm0.04$ a.u.) we integrate all cusps over the same velocity interval which is arbitrarily but consistently chosen to be $v\pm0.5$ a.u.

We have obtained total ELC cross sections from both our singles and coincidence measurements. In

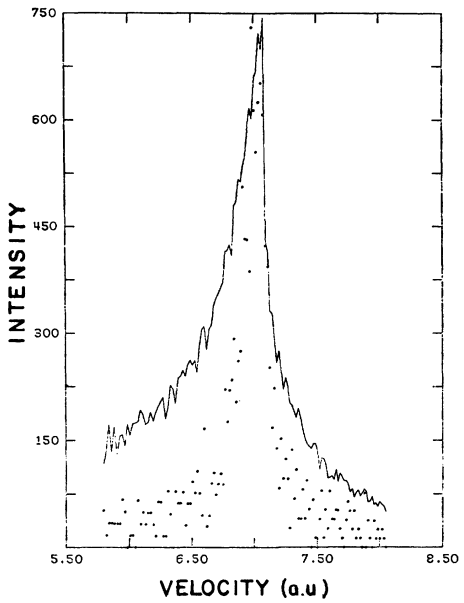

FIG. 20. Cusp for 20-MeV O^{7+} projectiles on Ar obtained in coincidence with O^{8+} (dots), overlaid with cusp containing all electrons not detected in coincidence with O^{8+} (solid line). The former is an ELC spectrum while the latter represents an ECC spectrum. Differences in ELC and ECC cusp shapes are obvious.

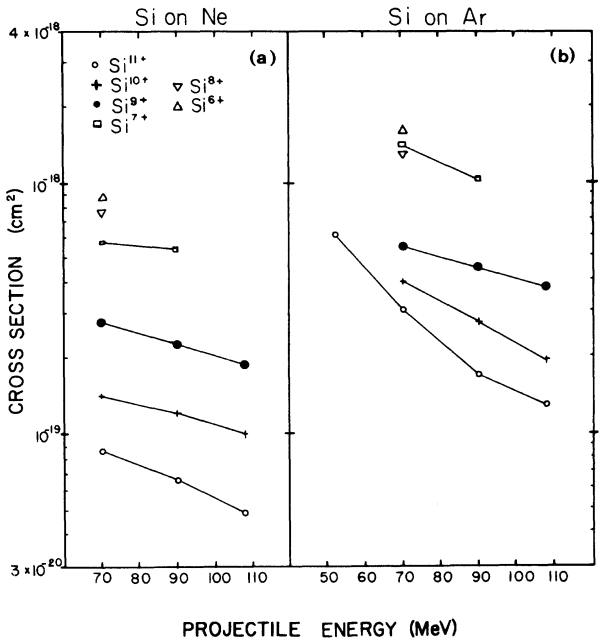

FIG. 21. Total electron loss to the continuum cross section into a cone of half angle $\theta_0 = 1.8°$ about the forward direction integrated over the velocity interval $v \pm 0.5$ a.u. for Si^{q+} projectiles on Ne and Ar targets.

the latter case we have summed over all final ion charge states. Figure 21 shows the total ELC cross section into a cone of half angle $\theta_0 = 1.8°$ about the forward direction integrated over the velocity interval $v \pm 0.5$ a.u. for Si^{q+} ions in Ne and Ar as a function of ion energy and ion charge state q. Figure 22 shows the total ELC cross sections for O^{q+} on Ar for the same θ_0 integrated over the same velocity interval. These cusp cross sections are compared to total electron-loss cross sections measured by Macdonald and Martin.[23] We find very similar energy and charge-state dependences.

For 20 and 30-MeV O^{q+} ($q = 4$, 5, 7) and C^{q+} ($q = 2$, 5) we have measured the spectrum of ELC electrons detected in coincidence with the charge state of the scattered ion. If the scattered ion charge state is $q-1$, only the detected ELC electron has been lost (single-electron loss). For scattered ion change states $q-2$ and $q-3$ one or two additional electrons were lost in the collision (double and triple electron loss).

Table V displays the ELC cusp cross sections associated with single, double, and triple electron loss for 20 and 30-MeV O^{q+} on Ar. These ELC cross sections are compared to single, double, and triple electron-loss cross sections as measured by Macdonald and Martin.[23] The trends with total number of electrons lost are similar for both sets of measurements. These trends are also displayed in Fig. 23 where the dependences of the ELC cross sections and the electron-loss cross sections of Ref. 23 on the scattered ion charge state for O^{4+} on Ar are plotted.

Table VI shows the ELC cusp cross section associated with single, double, and triple electron loss for 18.75-MeV C^{2+} on Ar and the total ELC cusp cross section for 18.75-MeV C^{5+} on Ar. As with all the above ELC cusps, θ_0 is 1.8° and the integration limits are $v \pm 0.5$ a.u.

D. Convoy electron production: Shapes and yields from singles measurements

"Convoy" electrons is the generic name that has been given to electrons that accompany ions as they emerge from solid targets. As remarked earlier, the ease of interchange of gaseous and solid targets in our apparatus while leaving all other geometrical and kinematic conditions fixed has permitted us to compare gaseous and solid target results under conditions where most systematic apparatus effects cancel to first order.

Our experiments with p, O, Si, and Ni projectiles

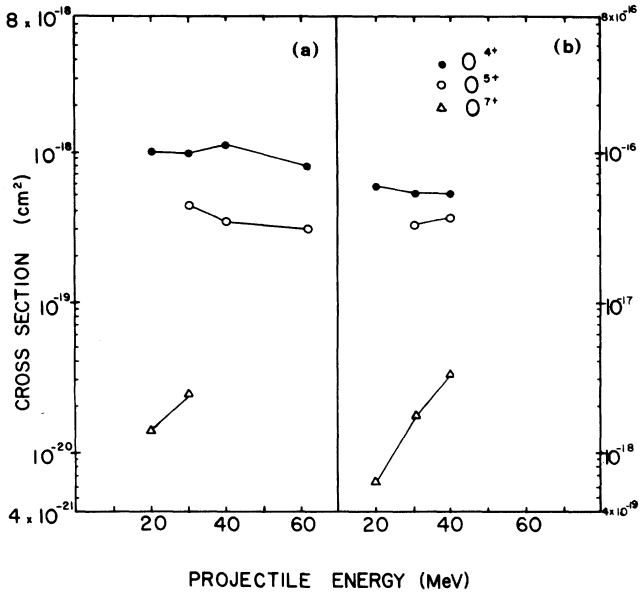

FIG. 22. Total ELC cross sections for O^{q+} projectiles on Ar targets. The integration limits are $v \pm 0.5$ a.u. and $\theta_0 = 1.8°$. (b) Total electron-loss cross sections measured by Macdonald and Martin (Ref. 23).

in the velocity range 6—14 a.u. on C, Al, and Au polycrystalline targets all yield convoy electron cusps of similar shape with the same FWHM of $= 0.25 \pm 0.02$ a.u, where $\theta_0 = 1.8°$ and the energy resolution of our analyzer is 1.4%. These results are at variance with all present theoretical considerations, as discussed in Sec. II.

One shortcoming of the above convoy experiments is that the electron-velocity distribution is averaged over all of the final projectile charge states. Guided by parallel experimental experience in our ECC studies, it became evident that a coincidence experiment specifying the relationship between the final charge state of the projectile and the electron-velocity distribution and yield would clarify the situation. A typical experimental result is shown in Fig. 24 for 12-MeV C^{2+} ions incident on a 40-μg/cm^2 Al target. A total, or singles, spectrum is shown together with electron-velocity spectra observed in coincidence with emergent C^{6+} ions ($\sim 25\%$ of the total), C^{4+} ions ($\sim 20\%$ of the total), and C^{3+} ions ($\sim 1.2\%$ of the total). The

TABLE V. ELC cross section ($\theta_0 = 1.8°$, integrated over the velocity interval $v \pm 0.5$ a.u.) associated with single-, double-, and triple-electron loss and single-, double-, and triple-electron-loss cross sections measured by Macdonald and Martin (Ref. 23) (MM) for O^{q+} projectiles on Ar.

	O^{q+}	20 MeV		30 MeV	
	q	σ_{ELC}(cm^2)	σ_{MM}(cm^2)	σ_{ELC}(cm^2)	σ_{MM}(cm^2)
Single-electron loss	4	7.9×10^{-19}	5×10^{-17}	7.9×10^{-19}	4×10^{-17}
	5		3×10^{-17}	4.1×10^{-19}	3×10^{-17}
	7	1.5×10^{-20}	6×10^{-19}	2.6×10^{-20}	2×10^{-18}
Double-electron loss	4	2.0×10^{-19}	9×10^{-18}	1.7×10^{-19}	1×10^{-18}
Triple-electron loss	4	1.3×10^{-20}	6×10^{-19}	2.0×10^{-21}	1×10^{-18}

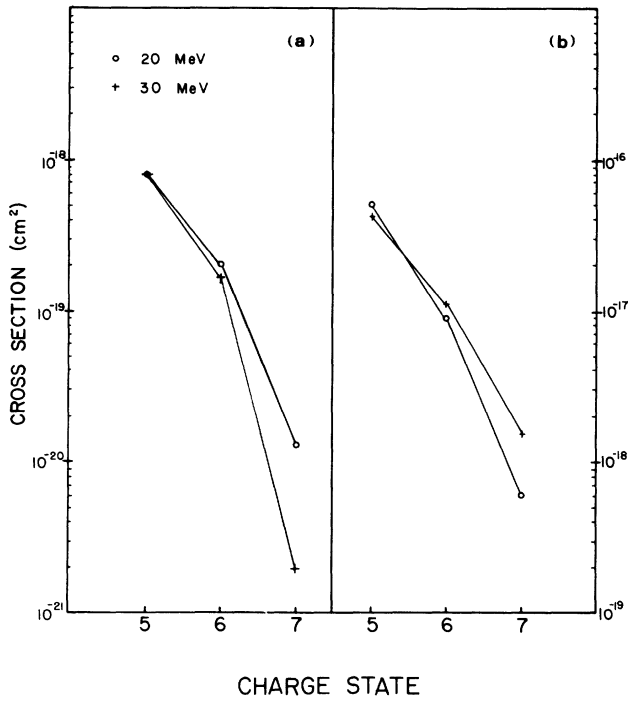

FIG. 23. (a) ELC cross sections for O^{4+} projectiles on Ar targets, measured in coincidence with the scattered-ion charge state. (b) Electron-loss cross sections for O^{4+} projectiles on Ar targets as a function of scattered-ion charge state as measured by Macdonald and Martin (Ref. 23). Scattered-ion charge states 5, 6, and 7 correspond to single-, double-, and triple-electron loss, respectively.

C^{5+} distribution accounted for 45% of the total and hence need not be shown. Lower final charge states were observed, but with intensities of less than 0.5% of the total. Hence reliable electron-velocity distributions (i.e., distributions corresponding to a true-to-accidental ratio greater than 5) could not be obtained.

Inspection of Fig. 24 leads to the conclusion that no differences in the velocity distribution of the convoy electrons are evident as the final charge state of the projectile is changed. In fact, the FWHM is the same for all the final charge states of the projectile. Changing the incident energy of the projectile (from 12 MeV to 33 MeV carbon), the charge state of the projectile, the atomic number of the projectile [carbon, oxygen, and silicon (all at 1 MeV/u)], or the target material (aluminum, carbon, and gold) does not alter the conclusion that to a good approximation the shape of the convoy electron-velocity distribution from solids is independent of the final projectile charge state. This statement also applies to crystalline targets. Recent theoretical considerations of Day[43] indicate a diffraction structure in the electron-velocity distribution and a Z dependence of the FWHM of approximately $Z^{1/4}$. No diffraction structure is observed in Fig. 24; however, it is unclear whether the present electron analyzer would be able to resolve the proposed structure.

TABLE VI. ELC cross section ($\theta_0=1.8°$, integrated over the velocity interval $v\pm0.5$ a.u.) associated with single-, double-, and triple-electron loss for 18.75-MeV C^{q+} on Ar.

	q	$\sigma_{ELC}(cm^2)$
Single-electron loss	2	2.5×10^{-18}
	5	4.2×10^{-20}
Double-electron loss	2	5.2×10^{-19}
Triple-electron loss	2	6.9×10^{-20}

We have obtained absolute values for the convoy electron yield defined as the number of convoy electrons per incident projectile from the measured convoy electron cusps. Absolute values for the restricted yield Y_R of convoy electrons emitted into a cone of half angle $\theta_0=1.8°$ about the forward

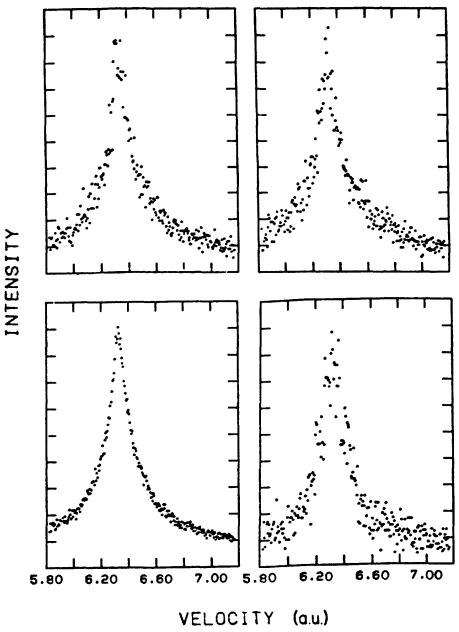

FIG. 24. The longitudinal velocity distribution of convoy electrons emerging from a solid when 12-MeV $^{12}_{6}C^{2+}$ is incident on a 40-μg/cm^2 Al target. The "singles" or noncoincident distribution is shown in the lower left-hand corner. The electron-velocity distributions in coincidence with the final charge state of C^{6+}, C^{4+}, and C^{3+} are shown in clockwise arrangement starting in the upper left-hand corner. The vertical scale (intensity) is arbitrarily normalized for each spectrum.

direction are obtained from the raw data of electron counts/channel using the following equation:

$$Y_R=\sum_j \frac{N_j(E_j)}{E_j}\Delta E_j \frac{\bar{q}}{Q}\frac{1.6\times10^{-10}}{\beta T_{\rm eff}(E_j)\theta_0^2} \times\frac{\text{electrons}}{\text{projectile deg}^2}\ . \tag{11}$$

In an analogous way we obtained ECC cross sections in Sec. IV A; the same symbols describe the same quantities. However, for solid targets $\bar{q}$ is the mean charge of the collected ions.

We sum over all channels corresponding to electron velocities v_e between $v\pm\gamma$. The widths of the convoy electron cusps do not scale linearly with velocity as in ECC but instead are found to be velocity independent. Since all measured cusps have a FWHM $\Gamma = 0.25 \pm 0.02$ a.u., we choose γ to be 0.5 a.u., twice the FWHM of the cusps.

For our published convoy electron yields the transmission/detection efficiency $T_{\rm eff}$ (E_j) of our apparatus is normalized to 100%. However, when normalizing our gaseous target data to the cross section for Ar L-Auger emission by Stolterfoht *et al.*[24] (see Sec. IV A) and assuming the values for $\Delta x = 5$ mm and $\theta_0 = 1.8°$, we find a transmission/detection efficiency of $\sim 50\%$ in agreement with the value obtained by Cranage and Lucas[14] for the same model CEM detector. This could increase all our published convoy yield data by approximately a factor of 2. Otherwise the uncertainties in the convoy electron yields and in the ECC and ELC cross sections are of the same magnitude (Sec. IV A).

Convoy electrons have a velocity distribution along the beam direction with FWHM Γ_l and a velocity distribution transverse to the beam direction with FWHM Γ_τ.

For solid targets we find $\Gamma_l = 0.25$ a.u. and infer $\Gamma_\tau = 1.8\ \Gamma_l = 0.45$ a.u., independent of the projectile velocity. (Here we have used the relationship $\Gamma_\tau \simeq 1.8\ \Gamma_l$, measured by Meckbach *et al.* in the lower-energy ion-solid collision studies.)

The total yield of convoy electrons may be estimated from an appropriate normalization and integration of the longitudinal velocity distribution. Our electron analyzer has a solid angle of acceptance centered on 0°, $\Delta\Omega$, and an energy resolution $\Delta E/E$ which fold the actual transverse and longitudinal velocity-distribution characteristics. Hence if the width and shape of the longitudinal and transverse velocity distributions were known accurately, we could obtain the total electron yield from a measurement of the yield in the longitudinal direction. They are currently known only approximately; Laubert *et al.*[32] use the following ansatz to permit total-yield estimation.

The velocity distribution in the longitudinal and transverse direction decreases exponentially, with half-widths $\Gamma_{l/2}$ and $\Gamma_{\tau/2}$, respectively. The total yield, in terms of the restricted yield Y_R, is

$$Y = Y_R \frac{1}{1-(1+Cv)\exp(-Cv)}\ , \tag{12}$$

where v is the projectile velocity and $C = 2\theta_0 \ln 2 / \Gamma_\tau$. Here θ_0 is expressed in radians and Γ_τ in a.u.

For $\theta_0 = 1°$, C takes the value 5.38×10^{-2}. (For solid targets we measure a higher fraction of the total electrons as the projectile velocity is increased than for ECC, where the corresponding cusps are wider.)

We find that the convoy electron yields Y_R and Y are independent of the incident charge state of the projectile and of the target thickness (the target thickness was changed by a factor of 2), but do

change for different target materials as well as with the energy and atomic number of the incident projectiles.

The data analyzed accordingly are shown in Fig. 25 for the various projectile-target combinations as a function of the incident particle energy. In the interest of clarity, only the oxygen projectile data are shown for all of the targets. For the H^+, Si^{q+}, and Ni^{q+} particles, only the C and Au target data are shown. The near linearity and parallelism of the similar target curves for each projectile shown in Fig. 25 suggest a common velocity dependence for the various projectiles, and approximate velocity-independent Z dependence. Indeed, we find that we can summarize all of our results by the empirical equation

$$Y = 1 \times 10^{-4} C(Z_T),\ Z^{2.75\pm0.2} E^{-2.25\pm0.1}, \qquad (13)$$

where Z is the atomic number of the incident particle of energy E in MeV/u; $C(Z_T)$ is a constant depending on the target material: C (Au) = 1.65, C (Ag) = 1.25, C (Al) = C (C) = 1.0. All the values have estimated uncertainites $\pm$ 0.15.

To our knowledge, the only other measurement of the yield of convoy electrons from solids is by Dettmann *et al.*[9] for 225-keV protons on carbon. The above equation predicts a result with 30% of their measurements. Meckbach *et al.*[17] report relative yield measurements for 200–500-keV protons on carbon and find an energy dependence of $\sim E^{-3.1}$ which is in reasonable agreement with our results.

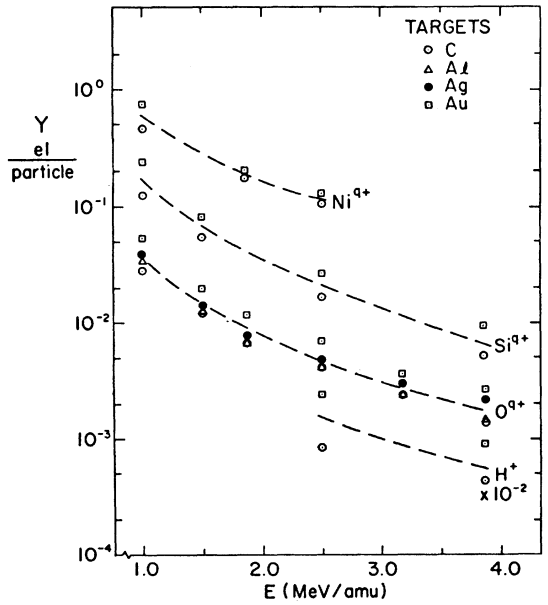

FIG. 25. The yield of convoy electrons for different target materials and different incident projectiles. The dashed lines are to guide the eye.

E. Convoy production measured in coincidence with emergent-ion charge

When we examine the yield of convoy electrons in coincidence with a particular final charge state of the projectile, we find the curious result that the convoy electron yield, per coincidently registered projectile, is independent of the final, projectile charge state. That is, the fraction of electrons coincident with a particular final charge state just mirrors by the fraction of projectiles having that particular charge state. If the atomic number and energy of the incident projectile or the target material is changed, we find that each coincident convoy electron yield varies in the same proportions as the noncoincident convoy electron yield.

These results strongly mitigate against the surface production of convoy electrons and suggest the bulk of the material as the origin of these electrons. To further explore this possibility, we utilized O^{6+}, O^{7+}, and O^{8+} beams traversing a Au single-crystal target and employed channeling techniques, where it is known that the incident ion charge state often remains intact (frozen) throughout the entire crystal passage (e.g., $\sim$ 80% of 2.5-MeV/u O^{8+} ions traversing the $\langle 110 \rangle$ direction will remain 8 + throughout a 300-μg/cm^2 gold crystal). The first experiments concerning convoy electron production by channeled ions were performed by Datz *et al.*[45] and by Dettmann *et al.*[46] We found that the shapes of the velocity distributions are independent of whether a channeling or random direction of a single-crystal target or a polycrystalline target was chosen and do not depend on q or q_e. However, in the channeling data, the yields which were found to be independent of the final projectile charge state for polycrystalline targets depend strongly on incident as well as exit charge state. Table VII presents in matrix form the yields per emergent ion for various incident q and exit q_e charge-state pairs, together with the corresponding measured charge-state fractions and coincident fraction values. It is immediately evident that convoy production for well-channeled ions is much suppressed, with the greatest suppression arising in the most open channel $\langle 110 \rangle$. It is also evident that the highest yields occur when the distance of approach to lattice sites is likely to be closest. The yield entries in Table VII can be

TABLE VII. Convoy electron yield (%) per emergent ion, for O^{8+} incident at 2.4 MeV/u on Au in the ⟨110⟩, ⟨100⟩, and random directions. The yield is normalized to the measured random yield of $\sim 3.8\times10^{-4}$ electrons/ion. The number in parentheses is the fraction (%) of emergent ions in state q_e.

q in	q_e out		8+	7+	6+
8+		$Y\langle110\rangle$	21 (68)	39 (28)	82 (4)
		$Y\langle100\rangle$	37 (59)	58 (35)	79 (6)
		$Y\langle\text{Rand}\rangle$	100 (26)	100 (59)	100 (15)
7+		$Y\langle110\rangle$	29 (42)	24 (51)	58 (7)
		$Y\langle100\rangle$	37 (52)	47 (42)	71 (6)
		$Y\langle\text{Rand}\rangle$	100 (25)	100 (60)	100 (15)
6+		$Y\langle110\rangle$	37 (31)	29 (42)	21 (27)
		$Y\langle100\rangle$	39 (49)	45 (42)	47 (9)
		$Y\langle\text{Rand}\rangle$	100 (27)	100 (57)	100 (16)

surprisingly well reproduced by postulating two classes of channeled ions: those that approach close enough to a lattice site (effective distance $\sim$ 0.65 Å) to produce a convoy electron with the high probability (equal to the random or polycrystalline rate); and those which remain at larger separations, producing convoys with negligibly low probability. Two immediate tests of this extreme assumption are well verified. First, the number 0.65 Å explains both the ⟨110⟩ and the ⟨100⟩ yield figures. Second, it happens that for Au atoms the 6*s* and 5*d* electrons have kinetic energies <10 eV. But the 5*p* and 4*f* electrons—which have binding energies of $\sim$ 250–460 eV and are therefore far more efficient at contributing to capture according to the Bohr $v_e \sim v$ matching criterion—have mean radii ranging from 0.60 to 0.28 Å. Therefore, the "magic" distance of 0.65 Å can be assigned a most plausible physical interpretation.

F. Model for convoy electron production in solids

The experimental evidence to date allows us to construct the following model for convoy electron production in solids. Convoy production is initiated in a close collision, most probably a single- or multiple-electron-capture event ($\sim 10^{-17}$ cm^2 capture cross section),[23] which, according to the work of Brown *et al.*,[47] is dominated by electron capture to excited states ($\gtrsim$ 90% of the time). The excited states most copiously populated have $n=2$ and 3, with populations of higher states possible at the $\gtrsim$ 10% level. Because binary-encounter theory predicts that e^- loss cross sections scale approximately as n^2 and because of the peak width and symmetry considerations noted above, we suggest that convoy production is initiated by capture(s) followed immediately by electron loss to the continuum. If the mean-free path for such dual events is $\gtrsim$ 250 Å, then several convoys per projectile would be produced in a solid a few thousand Å thick. Subsequent electron-electron scattering (elastic and inelastic) leads mainly to scattering into a wide range of angles, effectively extinguishing the convoy population, although it is possible that secondary elastic scattering would cause some unkown degree of repopulation. In any event, since the escape depth of $\sim$1-keV electrons is $\sim$10–20 Å, the net production of several convoy electrons per emergent ion is depleted by electron scattering to $\sim 10^{-2}$– 10^{-4} observable electrons per ion.

The skew of the electron-velocity distributions toward electron velocities $v_e > v$ can be qualitatively and quantitatively explained by considering the velocity dependence of the electron scattering cross section in solids.[48] We correct the observed cusp shape by a velocity-dependent factor ($\sim v^{-1.6}$) re-

flecting the exponential attenuation resulting from electron scattering within the bulk. The result of this procedure is shown in Fig. 26 for 16-MeV O^{3+} traversing carbon. The resultant symmetric, peak-normalized curve is similar to experimental electron-loss cusps from C^{q+} and O^{q+} traversing Ne and Ar (except for the additional low-energy Auger lines which appear in the cusp wings). Since no fitting procedure beyond over all peak normalization is used, the ability to quantitatively symmetrize the skewed peak is viewed as support for the bulk production of convoy electrons, a small fraction of which escape through the surface.

A curious and unexplained enigma remains unresolved by our otherwise very successful model. Three facts need to be reconciled. The free-electron-scattering data suggest that all of the observed convoy electrons—though they are produced throughout the bulk—originate within the final ~ 20 Å of passage through the target (otherwise they scatter out). Yet the mean-free path for projectile-ion charge changing under our conditions in C is ~ 200 Å, so that any ion traversing the final 20 Å of target has little likelihood of changing charge. The fundamental question posed is as follows: How can the correlation between emergent-ion charge-state and convoy electron yield be broken in a distance of ~ 20 Å? Unless the correlation is broken, it is very difficult to understand why the convoy electron yield is strongly dependent on projectile nuclear charge ($Z^{\sim 2.7}$), yet is independent of the emergent-ion charge (Z screened by zero to two tightly bound K electrons).

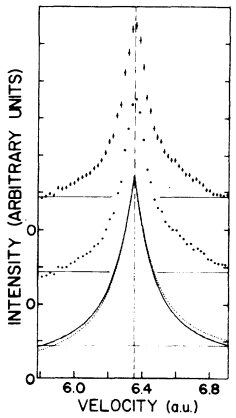

FIG. 26. Spectrum of convoy electrons emergent near 0° from 16-MeV O^{3+} ions traversing a 30-μg/cm^2 C foil. The upper data points are obtained from the raw spectrum (lower points), through a correction factor ($v_e^{-1.6}$) to account for the estimated velocity dependence of the electron escape depth. The lower curves represent respective fitted cusp shapes, which better display the degree of symmetrization produced.

V. CAPTURE AND LOSS TO RYDBERG AND SUPER-RYDBERG STATES IN GASES AND THE BEAM-FOIL CASCADE PROBLEM

As noted earlier in Sec. II A ionization (here ELC) can be thought of[3] as the natural continuation of excitation to a sequence of orbits of ever-increasing principal quantum number n into the continuum, provided an appropriate normalization of continuum states per unit bandwidth Δn relative to high-n Rydberg states is chosen. Similarly, ECC may be regarded as a smooth extension of bound-state electron capture to high Rydberg states, lying just below the continuum, into the continuum.[3] Paraphrasing the elaboration of these ideas in Ref. 11, an average projectile or target excitation cross section $d\sigma_n/dE_n$ is assumed to be a slowly varying function of E_n because excitation cross sections to states with high principal quantum numbers scale approximately as n^{-3}, exactly compensating for a density of states varying as n^3. For example, inelastic energy-loss measurements for protons carried out by Park and Schowengerdt[49] showed smooth continuation across the ionization limit. For electron capture, many experiments (e.g., those carried out by Hughes *et al.*[50]) indicate dominant capture to s states for protons traversing various gases as v is increased to $v >> v_0$, in accordance with prediction of a number of first Born approximation calculations of charge transfer.[1] (Note, however, that higher partial waves are important in second Born, double-scattering contributions to ECC at high velocities, as is demonstrated by our ECC cusp asymmetry data[51] for He.)

Following Ref. 11, we define a reduced cross section

$$\sigma_c = n^3 \sigma_n = n^3 \sum_{l,m} \sigma_{nlm} , \tag{14}$$

which is expected to be a slowly varying function of n. This scaling corresponds to the well-known n^{-3} scaling predicted by the Oppenheimer-Brinkman-Kramers (OBK) and Jackson-Schiff (JS) formulations of the first Born approximation to charge transfer.[1] Using L and P to denote labora-

tory and projectile frames, respectively, E_n to denote electron energy up to the ionization limit, and E_k that above it, continuation of the singly differential cross section above the ionization limit can be written

$$\left.\frac{d\sigma}{dE_n}\right|_P \simeq (\Delta E_n)^{-1} \sum_{E_n}^{E_n+\Delta E_n} (\sigma_{E_n}) \Bigg|_P$$

$$= \Delta E_n^{-1} \sum_{n}^{n+\Delta n} \sigma_n \cong \left.\frac{d\sigma}{dE_k}\right|_P . \quad (15)$$

The Coulomb potential energy levels are $E_n = (-Z^2/2n^2)\text{Ry}$, so that ΔE_n may be expressed as $(Z^2/n^3)\Delta n$ Ry. If n^3 is assumed constant over a small range Δn,

$$\left.\frac{d\sigma}{dE_n}\right|_P \cong \Delta E_n^{-1} \sum_{n}^{n+(n^3/Z^2\,\text{Ry})\Delta E_n} \frac{\sigma_c}{n^3} = \frac{\sigma_c}{Z^2}\,\text{Ry} . \quad (16)$$

Using the continuity relation

$$\left.\frac{d\sigma}{dE_k}\right|_P \cong \left.\frac{d\sigma}{dE_n}\right|_P = \sigma_c/Z^2\ \text{Ry},$$

σ_c can be reexpressed in laboratory-frame coordinates through the relation

$$\left.\frac{d\sigma}{dE_k}\right|_P = \left[\frac{d\sigma}{dE_e}\right]_L \frac{\Delta E_e}{\Delta E_k} , \quad (17)$$

where ΔE_e and ΔE_k, are corresponding energy windows in the two reference frames. For our analyzer, $\Delta E_e = 0.014E_e$, where E_e is the laboratory-frame electron kinetic energy. Consideration of the kinematics (near 0°) and of the apparatus resolution leads to $(\Delta E_e/\Delta E_k) = (16/0.014) = 1140$, so that a small energy window in the laboratory frame implies an extremely narrow band of energies in the projectile rest frame.

Accordingly, the laboratory-frame escape cone (half angle $\theta_{\max}$) for electrons corresponding to the window ΔE_k, is appreciably smaller than the acceptance cone (half angle $\theta_0 = 1.8°$ of the analyzer. A "filling factor" reduces the integration averaging over angles implied by

$$\left.\frac{d\sigma}{dE_e}\right|_L \cong \int_{\Delta\Omega_0} \frac{d^2\sigma}{dE_e d\Omega} \Bigg|_L d\Omega$$

to

$$\int_{\Delta\Omega_{\max}} \frac{d^2\sigma}{dE_e d\Omega} \Bigg|_L d\Omega . \quad (18)$$

The reduction factor R is not simply the ratio of the corresponding solid angles because of the strong $1/k$ weighting of the doubly differential cross section arising from the Coulomb wave-normalization factor[1] describing the cusp. Here k is the rest-frame electron-emission velocity. Accordingly, we write

$$\sigma_c = (d\sigma/dE_e)\,|_L (\Delta E_e/\Delta E_k)(Z^2\,\text{Ry})R , \quad (19)$$

where for our apparatus ($\Delta E/E = 0.014$, $\theta_0 = 1.8°$), $R \cong 0.059$, whereas for that of Rødbro and Andersen ($\Delta E/E = 0.01$, $\theta_0 = 0.36°$), it is $R \cong 0.23$. The value for R given by Rødbro and Andersen is 0.184, but this result appears to be low by $\sim 25\%$ owing to an integration error in computing the $(1/k)$-weighted "disk-shaped" resolution volume corresponding to their energy and angle windows.

Another adjustment, of inadequately known magnitude, is needed to account for the assumption of Rødbro and Anderson—an assumption also of the ECC theory of Dettmann, Harrison, and Lucas,[9] unjustified in retrospect—that the low-energy electrons are isotropically distributed in the projectile rest frame. It is evident from the work of Breinig *et al.*[51] as well as that of Meckbach *et al.*[40] and Macek *et al.*[39] that ECC cusps display forward-backward asymmetries characterized by finite p, d, . . ., partial waves in the scattering amplitude. The step observed by Breinig *et al.*[51] is a clear manifestation of the relative importance of at least one partial-wave amplitude whose angular dependence contains an odd Legendre polynomial (like a p wave).

Lacking the detailed experimental information concerning the velocity distribution in the projectile rest frame, which may be extracted from future angular distribution measurements near the forward direction, we will assume approximate isotropy in our subsequent discussion. However, the estimates of σ_c we give, while informative, can have only qualitative significance because of the unknown adequacy of the isotropy assumption. Finally, higher-order cusp-shape corrections such as those discussed by Meckbach *et al.*[40] have been ignored.

In discussing σ_c values derived from our experiments, we will focus our attention on He and C as prototypical gas and solid targets. Not only is He a simple, structureless target, but also the criterion $v >> v_0$ is best approached for this case (for our velocity range 6—18 a.u. v/v_0 has the range ~2—9). As noted earlier, there are strong qualitative similarities of the cusp shape and yield data

among the various polycrystalline and randomly oriented monocrystalline targets used. Accordingly, for solid targets, σ_c results for C only are presented. How to generate the corresponding results from the information for the Al, Ag, and Au targets used is also indicated.

A. Values of σ_c for ECC in helium

Equations (19) has been used to generate values of σ_c for both cases. For He, the needed values of $(d\sigma/dE_e)_L$ can be obtained from the data displayed in Fig. 15. Corresponding values of $(d\sigma/dE_e)_L$ are obtained by (1) multiplying the values of $(d\sigma/d\Omega)\,|_L$ shown by our experimental $\Delta\Omega$ of 3.1×10^{-3} sr; (2) using Eq. (5) to generate a value for $d\sigma_{\rm BK}(\theta_0)/\,dv$ at $v=0$ by finding the value of this quantity corresponding to the experimentally observed yield $\int_{v(1-\alpha)}^{v(1+\alpha)}(d\sigma/dv)\,dv$, where $\alpha = 0.04$; and (3) transforming $(d\sigma/dv)\,|_L$ to $(d\sigma/dE_e)_L$ by elementary kinematics.

Since the most extensive data is available for O^{8+} projectiles, we quote numerical values for this case. The results obtained are $\sigma_c \cong 30\times10^{-19}$ cm^2 (32 MeV), $\sim 10\times10^{-19}$ cm^2 (40 MeV), $\sim 2\times10^{-19}$ cm^2 (51 MeV), and $\sim 9\times10^{-20}$ cm^2 (66 MeV).

These results can be compared to the corresponding one-electron bound-state electron-capture cross section measurements of Macdonald and Martin,[23] who obtained values of σ_{87} of $\sim 3\times10^{-19}$ cm^2 (30 MeV) and $\sim 1\times10^{-19}$ cm^2 (40 MeV).

The apparent order of magnitude disagreement between σ_{87} and σ_c is superficial, and arises primarily from the breakdown of the n^3 scaling law when $v \gg v_0$ is not well satisfied, the breakdown being severe for low n. For our values of v/v_0, in the range 3–9, the n^3 scaling law would be expected to be well satisfied for $n \gg 1$, and, as we shall see, is apparently reasonably well satisfied for $n \gtrsim 10$ and moderately well satisfied for $n > 3$ or 4.

This conclusion is based upon OBK calculations carried out for O^{8+} projectiles (among others) traversing He at $\sim$ MeV/u by Guffey, Ellsworth, and Macdonald.[52] Their OBK cross-section estimates for 32-MeV O^{8+} in He yield $\sim$ 0.45 : 2.3 : 1.8 : 1.0 : 0.63 : 0.40 : 0.27 : 0.18 : 0.13 : 0.10 $\times10^{-19}$ cm^2 for $n = 1-10$, respectively. $\sum_n \sigma_{\rm OBK}$ then becomes $\sim 7.3\times10^{-19}$ cm^2, a factor of $\sim$ 2.4 greater than the experimentally determined values 3×10^{-19} cm^2. As it is well known that the OBK approximation consistently overestimates charge-transfer cross section in the Z, v range in question by a factor $\sim$ 3, but does appreciably better at reproducing v and n dependences, we simply ratio the OBK predictions by the factor 3/7.3 = 0.41 to produce predicted values of σ_n for 32-MeV O^{8+} in He of $\sim$ 0.19 : 0.95 : 0.74 : 0.41 : 0.26 : 0.17 : 0.11 : 0.74 : 0.054 : 0.041$\times10^{-19}$ cm^2 for $n = 1-10$, respectively. The corresponding "experimental" values of $n^3\sigma_n = \sigma_c$ thus become 0.19 : 7.6 : 20 : 26 : 33 : 37 : 34 : 38 : 39 : 41, respectively.

It thus appears that σ_c from our ECC experiments in He are gratifyingly accurate predictions of σ_c derived from the single-capture to bound-state measurements of Macdonald and Martin.[23] Table VIII summarizes the cross-section estimates just discussed.

The extent of agreement may be fortuitous. Beyond the experimental uncertainties in both sets of measurements, and the uncertainties in ECC line shape owing to the forward-backward asymmetries discussed above, the measurements of MacDonald and Martin[23] do not take account of an important effect—the strong correlation of bound-state capture with ECC. As seen in Sec. IV B many measurements tacitly assumed to correspond to pure bound-state capture processes, including those of Ref. 23, are actually compound measurements, because of the neglect of an unseen coincident ECC event occurring an unestablished frac-

TABLE VIII. Values of σ_c derived for 32-MeV O^{8+} traversing He.

E (MeV)	σ_c from ECC (this work) (cm^2)	σ_c from OBK scaling[a] of σ_{87}[b]									
		$n=1$	$n=2$	$n=3$	$n=4$	$n=5$	$n=6$	$n=7$	$n=8$	$n=9$	$n=10$
32	30×10^{-19}	0.19	7.6	20	26	33	37	34	38	39	41
40	10×10^{-19}	0.063	2.5	6.7	8.7	11	12	11	13	13	14

[a]Reference 49 (32 MeV).
[b]Reference 23 (30 MeV).

tion of the time.[41] While intuitively one expects such double-capture events (one bound capture plus one ECC) to be relatively rare in He *vis-à-vis* Ar, they cannot in principle be neglected.

B. Values of σ_c for convoy electron production in solid targets

The results of the above analysis, as summarized in Eq. (19), can easily be extended to solid targets as well. All of the same caveats concerning cusp-shape uncertainties apply.

Because the analysis of data pertaining to O^{q+} beams traversing carbon targets can easily be extended to other projectile-target combinations through use of the yield curves estimated by Laubert *et al.*,[32] we give here only results for O^{q+} ions in C over the range 1—4 MeV/u. In using these curves, it is important to note that they provide estimates of total yield Y in units of electrons per projectile particle per square degree, integrated over all electron energies and angles, extrapolated from the actual restricted yield measurements Y_R. These restricted-yield measurements sampled these quantities over a restricted regime (typically 1 a.u. and $\theta_0 = 1.8°$). To avoid major uncertainites in the extrapolation to Y we deal here only with the quantity

$$Y_R = Y[1-(1+Cv)\exp(-Cv)] ,$$

where $C = 0.0538\theta_0$ and the projectile velocity v is given in a.u. The quantity Y is adequately estimated from the empirical formula

$$Y = 1\times 10^{-4} C(Z_T) Z^{2.75} E^{-2.25} ,$$

as discussed in Sec. IV D.

Though, as noted earlier, convoy-electron production is thought to be a bulk effect, it is thought that typically one observes only those electrons which originate in the last few atomic layers because the remainder scatter out of the forward direction before escape. For convenience in generating effective values of σ_c for the solid-target case to compare with the gaseous-target case, we therefore re-express the yield result in terms of a cross section per target atom by dividing by the surface density of the target (in effect, making a "last-layer approximation" *not* to be taken literally). Our value of σ_c will therefore necessarily be an upper bound. The target material-dependent cross section σ corresponding to Y thus becomes $\sigma = 5\times 10^4\ C'(Z_T) Z^{2.75} E^{-2.25}$ b/atom, where $C'(\mathrm{C}) = 1.0$, $C'(\mathrm{Al}) = 1.3$, $C'(\mathrm{Ag}) = 1.7$, and $C'(\mathrm{Au}) = 2.2$. The actual measured yields Y_R correspond to the restricted cross section σ_R, where

$$\sigma_R = \sigma[1-(1+Cv)\exp(-Cv)] .$$

The results of this analysis for O^{q+} ions traversing carbon targets are displayed in Table IX. If one makes the plausible assumption that $\sigma_c = n^3\sigma_n$ is adequate for $n \gtrsim 4$ (in parallel with the He data), then approximate prediction of σ_n for oxygen, hydrogen, or other atoms emergent from C foils can be generated. Table X lists such estimates. In presenting the results, we postulate the existence of an effective charge Z_E seen by a Rydberg electron, presumably $Z_E \sim \bar{q}$, but the enigma posed by the emergent charge independence of the coincident convoy yield data renders the choice of Z_E ambiguous. Comparison of the entries for σ_c for O^{8+} on He with those O^{q+} on thin carbon targets shows that effective convoy electron-production rates in solids exceed those for He by about 3 or-

TABLE IX. Values of Y_R, σ_R, and $(Z/Z_E)^2\,\sigma_c$ for oxygen ions and protons traversing amorphous carbon targets. Values for σ_c can be estimated by multiplying column 3 entries by $(Z_E/Z)^2$, where Z_E is an assumed effective charge for convoy production (the effective charge seen by a super-Rydberg electron).

E (MeV/u)	Y_R (oxygen) (10^{-3}/projectile/deg^2)	σ_R (oxygen) (10^{-18} cm^2/deg^2)	$(Z/Z_E)^2 \times \sigma_c$ (oxygen) (10^{-15} cm^2)	Y_R (protons) (10^{-6}/projectile/deg^2)	σ_R (protons) (10^{-21} cm^2/deg^2)	σ_c (protons) (10^{-19} cm^2)
1.0	3.8	1.9	12.6	13.0	6.3	6.4
1.5	2.1	1.1	5.8	7.0	3.5	2.9
1.8	1.6	0.81	3.9	5.3	2.6	2.0
2.5	0.98	0.49	2.0	3.2	1.6	1.0
3.2	0.67	0.33	1.2	2.2	1.1	0.65
3.8	0.51	0.25	0.84	1.7	0.83	0.45

TABLE X. Estimated cross sections multiplied by $(Z/Z_E)^2$ for Rydberg state production from O^{q+}, H^+ ions incident on C foils at 1 MeV/u. Cross sections for a chosen effective charge Z_E can be obtained by multiplying the entries by $(Z_E/Z)^2$.

n	O^{q+} incident (Mb)	H^+ incident (b)
4	200	10000
5	100	5100
6	58	3000
7	37	1900
8	25	1300
9	17	880
10	13	640
20	1.6	80
30	0.47	24
40	0.20	10
50	0.10	5.1
60	0.058	3.0
70	0.037	1.9
80	0.025	1.3
90	0.017	0.88
100	0.013	0.64

ders of magnitude (and by 1–2 orders of magnitude for Ne and Ar targets). This high convoy production rate can be used to derive predicted yields of Rydberg and high Rydberg states through the same scaling $\sigma_c = n^3\sigma_n$ if once again continuity across the ionization limit is invoked. For O^{q+} and proton beams at 1 MeV/u, the band $\Delta n = 4-10$ accounts for a cross section of $\sim$ 440 Mb and $\sim$ 23 kb, respectively; the band $n = 10-20$ for $\sim$ 47 Mb and $\sim$ 24 kb, respectively ; $n = 20-50$ for $\sim$13 Mb and $\sim$0.7 Kb; $n = 50-100$ for $\sim$1.9 Mb and $\sim$96 b; and $n = 100-\infty$ 0.6 Mb and $\sim$32 b. For $n \geq 10$, the approximation

$$\sum_{n}^{n+\Delta n} \sigma_n = \sigma_c \int_n^{n+\Delta n} \frac{dx}{x^3}$$

$$= \sigma_c/2[1/n^2 - 1/(n+\Delta n)^2]$$

has been used. Very similar estimates are easy to generate for other Z,v values in other targets using the $Z^{2.75}$, $E^{-2.25}$ scalings of the expressions for σ_R and σ given above.

A very well-known, systematic problem affecting lifetime measurements using the beam-foil technique is associated with estimating the amount of cascade feeding of lower levels repopulated from higher levels as a function of time. Initial population estimates enter at the starting point of such calculations. The degree of success of application of the population estimates just provided remains to be worked out. For this purpose, it is important to specify σ_{nl}, not just σ_n. The degree of dominance of s-state production for arbitrary Z,v is not known to the authors. However, for high-n levels, both stray fields as well as those associated with analysis of ECC, ELC electron spectra using the present experimental techniques are sufficient to create statistical mixture of l states through Stark mixing, and in the case of very high n-state populations, to cause appreciable field ionization. Since the weight of evidence is that n-state populations continue smoothly through the ionization limit, and that $\sigma_c = n^3\sigma_n$ is a useful estimate both above and below the ionization limit, it would appear that the question of whether a particular high Rydberg state is slightly bound or slightly unbound is only of minor importance in interpreting ECC, ELC, and convoy spectrum shapes and yields.

ACKNOWLEDGMENTS

We are happy to acknowledge the excellent assistance of the staffs of the ORNL, BNL, and LBL accelerator facilities used in this work. The accelerators used were the ORNL tandem accelerator, the BNL tandem accelerators, and the Berkeley Super-HILAC accelerator. This work was supported in part by the National Science Foundation, the U. S. Office of Naval Research, and the East Carolina Research Council. Three of us (G. D. A., S. D., and S. O.) acknowledge the support of the Fundamental Interactions Branch, Division of Chemical Sciences, Office of Basic Energy Sciences, U. S. Department of Energy.

*Deceased.

[1] R. Shakeshaft and L. Spruch, Rev. Mod. Phys. 51, 369 (1979); Phys. Rev. Lett. 41, 1037 (1978).

[2] I. A. Sellin, J. Phys. (Paris) Colloq. Suppl. No. 2, 40, C1–225 (1978).

[3] M. E. Rudd and J. Macek, Case Stud. At. Phys. 3, 125 (1972).

[4] R. Shakeshaft, Phys. Rev. A 18, 1930 (1978).

[5]J. Macek, Phys. Rev. A 1, 235 (1970).
[6]W. J. B. Oldham, Jr., Phys. Rev. A 140, 1477 (1965); 161, 1 (1967).
[7]M. M. Duncan, M. G. Menendez, F. L. Eisele, and J. Macek, Phys. Rev. A 15, 1785 (1977); M. W. Lucas, Proceedings of the Workshop on Physics with Fast Molecular-Ion Beams, August 1979, edited by D. S. Gemmel, p. 291 (unpublished).
[8]A. Salin, J. Phys. B 2, 631 (1969); B 2, 1225 (1969); B 5, 979 (1972).
[9]K. Dettmann, K. G. Harrison, and M. W. Lucas, J. Phys. B 7, 269 (1974).
[10]V. H. Ponce and W. Meckbach, Comments At. Mol. Phys. (in press).
[11]M. Rødbro and F. D. Andersen, J. Phys. B 12, 2883 (1979).
[12]G. B. Crooks and M. E. Rudd, Phys. Rev. Lett. 25, 1599 (1970).
[13]K. G. Harrison and M. W. Lucas, Phys. Lett. 33A, 142 (1970), and 35A, 402 (1971).
[14]R. W. Cranage and M. W. Lucas, J. Phys. B 9, 445 (1976).
[15]R. Strong and M. W. Lucas, Phys. Rev. Lett. 39, 1349 (1977); M. W. Lucas and R. Strong, Bull. Am. Phys. Soc. 23, 1087 (1978).
[16]M. G. Menendez and M. M. Duncan, in *Beam-Foil Spectroscopy*, edited by I. A. Sellin and D. J. Pegg (Plenum, New York, 1976), Vol. 2, p. 623; M. G. Menendez and M.M. Duncan, Phys. Lett. 54A, 409 (1975); Phys. Rev. A 13, 566 (1976); Phys. Lett. 56A, 177 (1976); Phys. Rev. Lett. 40, 1642 (1978); M. G. Menendez, M. M. Duncan, F. L. Eisele, and B. R. Junker, Phys. Rev. A 15, 80 (1977); M. M. Duncan and M. G. Menendez, *ibid.* 16, 1799 (1977).
[17]W. Meckbach, N. Arista, and W. Brandt, Phys. Lett. 65A, 113 (1978); W. Meckbach, K. C. R. Chiu, H. H. Brongersma, and J. W. McGowan, J. Phys. B 10, 3255 (1977), and references therein, and W. Meckbach and R. A. Baragiola, *Inelastic Ion-Surface Collisons*, edited by Tolk *et al.* (Academic, New York, 1977), pp. 283–308.
[18]K. C. R. Chiu, J. W. McGowan, and J. B. A. Mitchell, J. Phys. B 11, L117 (1978); K. C. R. Chiu, W. Meckbach, G. Sanchez Sarmiento, and J. W. McGowan, *ibid.* 12, L147 (1979).
[19]W. Steckelmacher, R. Strong, M. N. Khan, and M. W. Lucas, J. Phys. B 11, 2711 (1978); W. Steckelmacher and M. W. Lucas, *ibid.* 12, L152 (1979).
[20]W. Brandt and R. H. Ritchie, Phys. Lett. 62A 374 (1977).
[21]W. Steckelmacher and M. W. Lucas, J. Phys. E 12, 961 (1979).
[22]C. R. Vane, I. A. Sellin, M. Suter, G. Alton, S. B. Elston, P. M. Griffin, and R. S. Thoe, Phys. Rev. Lett. 40, 1020 (1978).
[23]J. R. Macdonald and F. W. Martin, Phys. Rev. A 4, 1965 (1971).
[24]N. Stolterfoht, D. Schneider, and P. Ziem, Phys. Rev. A 10, 81 (1974).
[25]M. E. Rudd, Phys. Rev. A 10, 518 (1974).
[26]F. Drepper and J. S. Briggs, J. Phys. B 9, 2063 (1976).
[27]J. S. Briggs and F. Drepper, J. Phys. B 11, 4033 (1978).
[28]M. Suter, C. R. Vane, I. A. Sellin, S. B. Elston, G. D. Alton, R. S. Thoe, and R. Laubert, Phys. Rev. Lett. 41, 399 (1978).
[29]W. Meckbach *et al.* (private communciation) and unpublished.
[30]M. Suter, C. R. Vane, S. B. Elston, G. D. Alton, P. M. Griffin, R. S. Thoe, L. Williams, I. A. Sellin, and R. Laubert, Z. Phys. A 289, 433 (1979).
[31]S. Bashkin and J. O. Stoner, Jr., *Atomic Energy Levels and Grotian Diagrams* (North-Holland/American Elsevier, Amsterdam/New York, 1975).
[32]R. Laubert, I. A. Sellin, C. R. Vane, M. Suter, S. B. Elston, G. D. Alton, and R. S. Thoe, Nucl. Instrum. Methods 170, 557 (1980), and references therein.
[33]C. R. Vane, IEEE Trans. Nucl. Sci. NS-26, 1078 (1979).
[34]V. N. Neelavathi, R. H. Ritchie, and W. Brandt, Phys. Rev. Lett. 33, 302 (1974); M. H. Day, *ibid.* 44, 752 (1980).
[35]R. Laubert, S. Huldt, M. Breinig, L. Liljeby, S. B. Elston, R. S. Thoe, and I. A. Sellin, J. Phys. B 14, 859 (1981); R. Laubert, I. A. Sellin, C. R. Vane, M. Suter, S. B. Elston, G. D. Alton, and R. S. Thoe, Phys. Rev. Lett. 41, 712 (1978).
[36]S. Datz, F. W. Martin, C. D. Moak, B. R. Appleton, and L. B. Bridwell, in *Atomic Collisions in Solids IV*, edited by S. Andersen (Gordon and Breach, New York, 1972), p. 87.
[37]F. T. Chan and J. Eichler, Phys. Rev. A 20, 367 (1979).
[38]M. W. Lucas, W. Steckelmacher, J. Macek, and J. E. Potter, J. Phys. B. 13, 4833 (1980).
[39]J. Macek, J. E. Potter, M. M. Duncan, M. G. Menendez, M. W. Lucas, and W. Steckelmacher, Phys. Rev. Lett. 46, 1571 (1981).
[40]W. Meckbach, I. B. Nemirovsky, and C. R. Garibotti, Phys. Rev. A (in press).
[41]C. R. Vane, I. A. Sellin, S. B. Elston, M. Suter, R. S. Thoe, G. D. Alton, S. D. Berry, and G. A. Glass, Phys. Rev. Lett. 43, 1388 (1979).
[42]M. Breing, M. M. Schauer, I. A. Selllin, S. B. Elston, C. R. Vane, R. S. Thoe, and M. Suter, J. Phys. B 14, L291 (1981).
[43]M. H. Day, J. Phys. B 13, L65 (1980).
[44]J. S. Briggs and M. H. Day, J. Phys. B 13, 4797 (1980).
[45]S. Datz, Nucl. Instrum. Methods 132, 16 (1976); S. Datz, B. R. Appleton, J. A. Biggerstaff, T. S. Noggle, and H. Verbeek, Book of Abstracts, VIth International Conference on Atomic Collisions in Solids, Amsterdam, 1975 (unpublished), p. 162.
[46]K. Dettmann, M. N. Khan, and M. W. Lucas, J. Phys. C 9, 1879 (1976); M. N. Khan and M. W. Lu-

cas, Book of Abstracts, VIth International Conference on Atomic Collisions in Solids, Amsterdam, 1975 (unpublished), p. 160; Phys. Rev. B 19, 5578 (1979).

[47]M. D. Brown, L. D. Ellsworth, J. A. Guffey, T. Chiao, E. W. Pettus, L. M. Winters, and J. R. Macdonald, Phys. Rev. A 10, 1255 (1974).

[48]J. C. Ashley, C. J. Tung, and R. H. Ritchie, Surf. Sci. 81, 409 (1979), and references therein.

[49]J. T. Park and F. D. Schowengerdt, Phys. Rev. 185, 152 (1969).

[50]R. H. Hughes, H. R. Dawson, and B. M. Doughty, Phys. Rev. 164, 166 (1967); R. H. Hughes, H. R. Dawson, B. M. Doughty, D. B. Kay, and C. A. Stigers, Phys. Rev. 146, 53 (1966); R. H. Hughes, C. A. Stigers, B. M. Doughty, and E. D. Stokes, Phys. Rev. A 1, 1424 (1970).

[51]M. Breinig, S. Elston, I. Sellin, L. Liljeby, R. Thoe, C. R. Vane, H. Gould, R. Marrus, and R. Laubert, Phys. Rev. Lett. 45, 1689 (1980).

[52]J. A. Guffey, L. D. Ellsworth, and J. R. Macdonald, Phys. Rev. A 15, 1863 (1977).